Lithos xxx (2009) xxx–xxx

Contents lists available at ScienceDirect

Lithos

journal homepage: www.elsevier.com/locate/lithos

Alpine tectonics in the Calabrian–Peloritan belt (southern Italy): New $^{40}Ar/^{39}Ar$ data in the Aspromonte Massif area

Thomas Heymes [a,*], Patrick Monié [b], Nicolas Arnaud [b], Arnaud Pêcher [a], Jean-Pierre Bouillin [a], Roberto Compagnoni [c]

[a] LGCA, UMR CNRS 5025, Université Joseph Fourier, Maison des Géosciences, BP 53, 38041 Grenoble, France
[b] Géosciences Montpellier, UMR CNRS 5243, Université Montpellier II, Place Bataillon, 34095 Montpellier Cedex 5, France
[c] DSMP, Università degli Studi di Torino, Via Valperga Caluso 35, 10125 Torino, Italy

ARTICLE INFO

Article history:
Received 27 March 2009
Accepted 9 October 2009
Available online xxxx

Keywords:
Western Mediterranean
Calabrian–Peloritan belt
Alpine convergence/extension
Exhumation
$^{40}Ar/^{39}Ar$ dating
Mylonitic shear zones.

ABSTRACT

This study provides new $^{40}Ar/^{39}Ar$ geochronological constraints on the age of the Alpine tectonics in the Aspromonte Massif (southern part of the Calabrian–Peloritan belt). This massif exposes the upper units of the Calabride Complex which originated from the European continental margin. The Calabride Complex was incorporated in the Alpine orogenic wedge and then integrated into the Apennines and Maghrebides fold-and-thrust belts. Throughout the Calabride Complex there is evidence for a two stage tectonic history, which remains however rather poorly dated: Alpine nappe stacking is followed by extensional reworking along the former thrust contacts or along new detachment surfaces. Our new ages suggest that exhumation of the uppermost units, which accompanied nappe stacking, probably started at 45 Ma and that the deepest units were almost completely exhumed at 33 Ma. This kinematics probably corresponds to syn-orogenic extension while the end of exhumation is clearly related to the extensional tectonics dated at 28.6 Ma along detachment structures.

Our geochronological data reveal a very short lag time between accretional and extensional processes in this part of the Mediterranean Alpine orogenic belt. The direction of extension, when the units are restored to their initial position (i.e. before the opening of the Western Mediterranean basins and the bending of the arc) is NNE–SSW. Such a direction does not fit with the eastward slab-retreat model generally put forward to explain extension in the Western Mediterranean. In contrast, we provide evidence for roughly N–S middle Oligocene extension in the accretionary prism, not previously described in this part of the Mediterranean domain.

1. Introduction

In the Western Mediterranean, thinned continental crust or oceanic basins are surrounded by an almost continuous Alpine orogenic belt. Several basins can be distinguished: the Ligurian–Provençal Basin between the south-European margin and the Corsica–Sardinia block, the North-Algerian Basin and the adjacent Alboran Sea, which are connected eastward through the Sardinia Channel with the Tyrrhenian Basin (Fig. 1). The opening of these extensional basins occurred within the European Plate, i.e. in a back-arc position with respect to the Tethyan northwest-directed subduction zone (e.g. Rehault et al., 1984; Vigliotti and Langenheim, 1995). Due to the fragmentation of the Alpine orogenic belt constructed during the convergence of the African, Apulian and Eurasian plates, the timing, initial location and kinematic direction of the extension, as well as the opening mechanisms are still poorly constrained. According to Alvarez (1976), Bouillin (1986), Stampfli et al. (1998) or Schettino and Turco (2006), the Calabrian–Peloritan Arc, the Kabylian massifs, the Moroccan Rif and the Betic Cordilleras are segments of the southern-European paleomargin (block AlKaPeCa), adjoining the Corsica–Sardinia block and were transported to their present position during opening of the Western Mediterranean basins.

Progressive eastward slab retreat is classically put forward to explain this extension (e.g. Malinverno and Ryan, 1986; Royden, 1993; Lonergan and White, 1997; Doglioni et al., 1997; Brunet et al., 2000; Jolivet and Faccenna, 2000; Mascle et al., 2001, Faccenna et al., 2004; Rosenbaum and Lister, 2004) in a geodynamic context controlled since the Upper Eocene by bulk N–S directed Africa–Eurasia convergence (e.g. Dewey et al., 1989; Rosenbaum et al., 2002). In the Tyrrhenian Sea area, this model is supported by the progressive eastward younging of sedimentary basins and volcanics (Jolivet et al., 1998; Brunet et al., 2000). In addition, in the two lateral ends of the

* Corresponding author. Present address: LGCA, UMR 5025, Université de Savoie, 73376 Le Bourget du Lac Cedex, France. Tel.: +33 4 79 75 87 15; fax: +33 4 79 75 87 77.
E-mail addresses: Thomas.Heymes@univ-savoie.fr (T. Heymes), Patrick.Monie@gm.univ-montp2.fr (P. Monié), Nicolas.Arnaud@gm.univ-montp2.fr (N. Arnaud), Arnaud.Pecher@ujf-grenoble.fr (A. Pêcher), Jean-Pierre.Bouillin@ujf-grenoble.fr (J.-P. Bouillin), Roberto.Compagnoni@unito.it (R. Compagnoni).

0024-4937/$ – see front matter © 2009 Elsevier B.V. All rights reserved.
doi:10.1016/j.lithos.2009.10.011

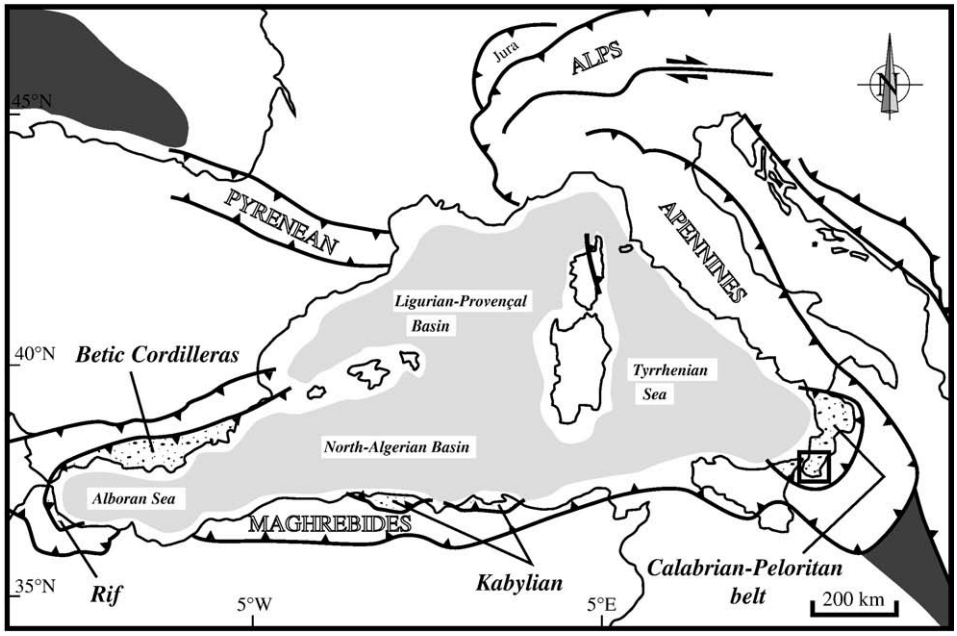

Fig. 1. Simplified tectonic map of the Western Mediterranean region (after Platt, 2007). Dark grey shading: Mesozoic oceanic basins; light grey shading: thinned continental crust and oceanic domains opened during Cenozoic times. The main Alpine tectonic contacts are reported as well as the corresponding orogenic belts. The study area is shown by the black box.

Western Mediterranean, tomographic images of the mantle and earthquake locations show the Tethyan oceanic slab plunging eastward in the Gibraltar area (Gutscher et al., 2002) and north-westward in the Calabrian–Peloritan Arc area (Lucente et al., 1999; Faccenna et al., 2001; Lucente et al., 2006), respectively. These two geometries fit well with the slab orientation deduced from the slab-retreat model.

Geodynamic reconstructions suggest that extension started during the early Oligocene with the opening of the Ligurian–Provençal Basin, accommodated by counterclockwise rotation of the Corsica–Sardinia block (Westphal et al., 1976; Rehault et al., 1984; Bois, 1993; Hippolyte et al., 1993; Vigliotti and Langenheim, 1995; Benedicto et al., 1996; Rollet et al., 2002). Closer to the former European southern paleomargin, in the Calabrian–Peloritan belt, Platt and Compagnoni (1990) and Rossetti et al. (2004) reported Oligocene–Miocene extensional tectonics, the geometry of which has recently been clarified by Heymes et al. (2008): all across the Calabrian–Peloritan belt, its direction is NNE–SSW, perpendicular to the SE direction assumed for the Tethyan slab retreat. The new $^{40}Ar/^{39}Ar$ data obtained in the southern part of the Calabrian–Peloritan belt, where only very few ages are available for the Alpine tectonics, yield more geochronological constraints to the onset of the post-orogenic extension in this segment of the southern-European margin.

2. Geological setting

2.1. The Calabrian–Peloritan belt

Our data were collected in the Aspromonte Massif, the southernmost part of peninsular Italy (Fig. 2). This massif is part of the Calabrian–Peloritan belt, the link between the Apennines in Italy and the Maghrebides in Sicily and in North Africa. The Calabrian–Peloritan belt is composed of a nappe pile of metamorphic rocks comprising ophiolitic units with their Mesozoic-Cenozoic sedimentary cover derived from the Tethyan oceanic domain (the "Liguride Complex"; Ogniben, 1973), which are overlain by a large sheet of pre-Alpine continental-derived metamorphics with local remnants of a Mesozoic–Cenozoic cover (the "Calabride Complex"; Ogniben, 1973). The arc-shape of the Calabrian–Peloritan belt has been acquired during opening of the Tyrrhenian basin since the Tortonian (e.g. Kastens et al., 1988; Rosenbaum and Lister, 2004).

Some authors have suggested that the tectonic units forming the Calabride Complex originated either from the northern margin of the African plate (e.g., Amodio-Morelli et al., 1976; Bonardi et al., 2003) or from a microplate sandwiched between the African and the European plates (e.g., Cello et al., 1996; Liberi et al., 2006). However, on the basis of geometric reconstructions of the Mesozoic sedimentary sequences, meso- and microstructural observations (fold orientations, stretching lineations, shear-sense indicators), and paleomagnetic measurements, the tectonic units forming the Calabride Complex are generally considered to have originated from the southern-European margin (e.g. Bouillin, 1984; Bouillin, 1986; Knott, 1987; Dietricht, 1988; Bouillin et al., 1988; Bouillin and Bellomo, 1990; Bouillin et al., 1992; Gueguen et al., 1998; Bouillin et al., 1999; Faccenna et al., 2001; Rosenbaum and Lister, 2004). According to this model, plate kinematics resulted in the progressive closure of the Tethyan oceanic domain during the Eocene, accommodated by northwest-directed subduction underneath the southern-European continental margin. The tectonic pile of the Calabrian–Peloritan belt has been built up during this convergence and transported onto the African–Apulian paleomargin.

In the oceanic-derived Liguride Complex of northern Calabria, this tectonic evolution is accompanied by an Alpine blueschist-facies metamorphic imprint (e.g. Dubois, 1970; Rossetti et al., 2001; Rossetti et al., 2004) resulting from burial of the Tethyan oceanic rocks in the subduction channel. In the Calabride Complex, the Alpine metamorphic imprint is mainly localized along the main tectonic contacts, where it partially or totally obliterates the Hercynian metamorphic parageneses. This Alpine metamorphic evolution ends with a greenschist-facies overprint associated with extensional reworking of the tectonic pile. This tectonic evolution, marked by the superposition of shortening and extension phases, is considered by Rossetti et al. (2004) as a local witness of the Cenozoic Western Mediterranean geodynamic evolution. In southern Calabria, a similar tectonometamorphic evolution has been described according to the lines of evidence reported below.

2.2. The tectonometamorphic pile of southern Calabria

Both in the Aspromonte Massif of southern Calabria and in the adjacent Peloritan Mountains of Sicily, only the uppermost part of the Calabride Complex can be observed. In the Aspromonte Massif, three

Please cite this article as: Heymes, T., et al., Alpine tectonics in the Calabrian–Peloritan belt (southern Italy): New $^{40}Ar/^{39}Ar$ data in the Aspromonte Massif area, Lithos (2009), doi:10.1016/j.lithos.2009.10.011

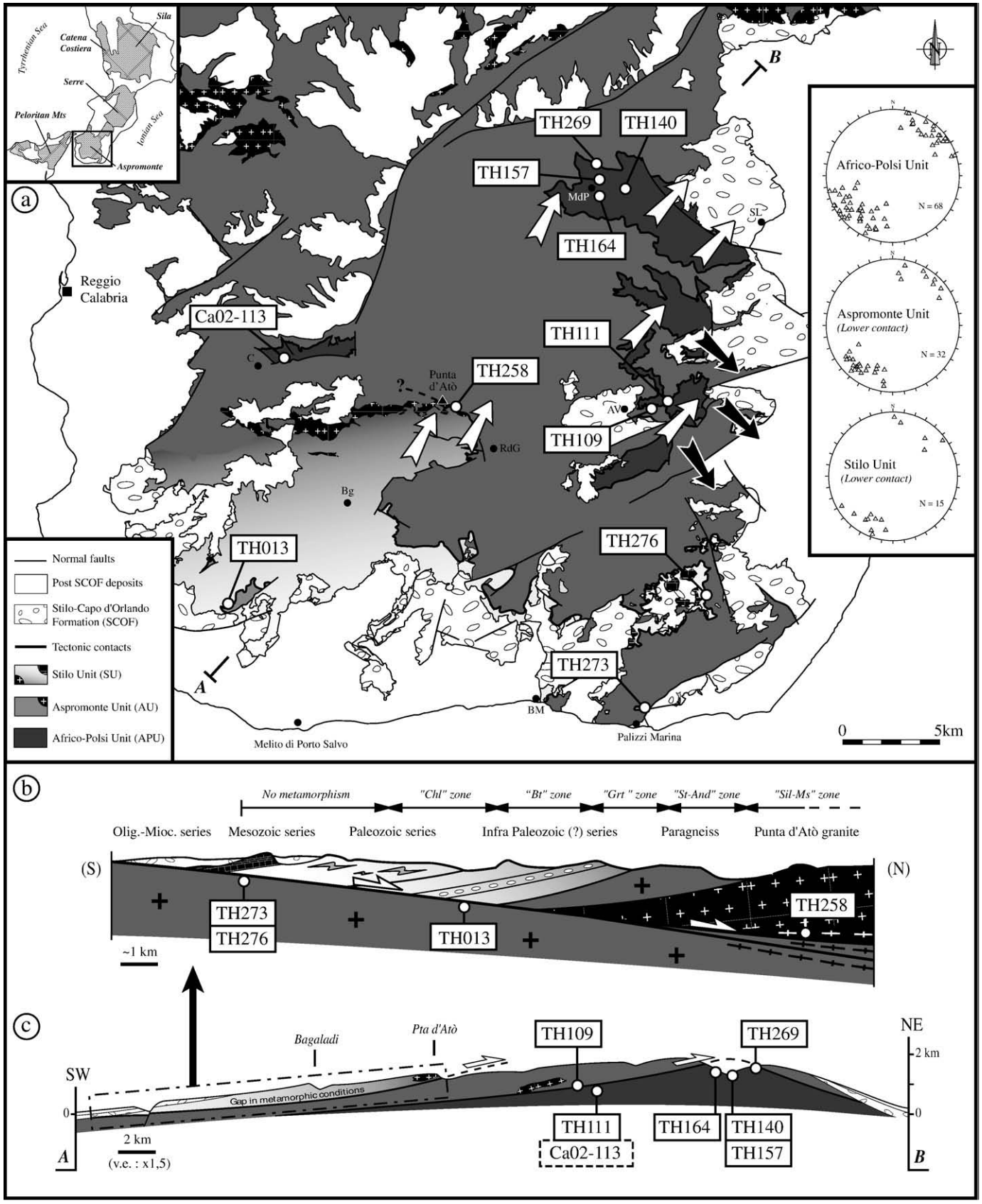

Fig. 2. (a) Structural map of the Aspromonte Massif (modified after Pezzino and Puglisi, 1980; Bonardi et al., 1984; Ortolano et al., 2005 and Heymes et al., 2008). The large arrows indicate the transport direction of the top of the tectonic pile: black arrows refer to the stacking phase (D1), and white arrows to the extensional reworking phase (D2). Stereoplots show the stretching lineation associated with the displacement direction during the D2 event (after Heymes et al., 2008). (b) and (c): Schematic cross-sections showing the detailed geometric organization of Stilo and Aspromonte units before tilting and erosion (b) and the present-day tilted tectonic architecture of the Aspromonte Massif (vertical exaggeration: 1.5) (c). The studied samples are located both on the map and cross-sections. Bg: Bagaladi; C: Cardeto; RdG: Roccaforte del Greco; BM: Bova Marina; AV: Africo-Vecchio; SL: San Luca; MdP: Madonna dei Polsi.

Please cite this article as: Heymes, T., et al., Alpine tectonics in the Calabrian–Peloritan belt (southern Italy): New $^{40}Ar/^{39}Ar$ data in the Aspromonte Massif area, Lithos (2009), doi:10.1016/j.lithos.2009.10.011

tectonometamorphic units are usually recognized, which are from bottom to top and from north to south: the Africo-Polsi Unit, the Aspromonte Unit and the Stilo Unit (Bonardi et al., 1979; Pezzino et al., 1992; Heymes et al., 2008) (Fig. 2).

The Africo-Polsi Unit, as defined by Heymes et al. (2008), crops out in the northeastern part of the massif and in a small tectonic window in its northwestern part (Bonardi et al., 1979; Pezzino et al., 1990; Ortolano et al., 2005). It consists of infra-Mesozoic metasediments and metavolcanics affected by a polyphase metamorphic history. Remnants of a probably Hercynian metamorphic assemblage are locally preserved (see Sections 3.1 and 4.2.1) and the main foliation is generally considered as Alpine. According to Ortolano et al. (2005) and Cirrincione et al. (2008), the lower unit of the Aspromonte nappe pile recorded an Alpine prograde metamorphic imprint reaching peak pressure–temperature conditions around 11.2–12.4 kbar and 540–570 °C, increasing slightly from south to north. *PT* estimates for the subsequent retrograde phase suggest an initial adiabatic decompression followed by relatively rapid final exhumation.

The Africo-Polsi Unit is tectonically overlain along a sub-horizontal contact by the Aspromonte Unit (Bonardi et al., 1979) which is mainly composed of paragneiss and orthogneiss, affected by homogeneous Hercynian low-pressure amphibolite-facies metamorphism (*PT* conditions for the peak of Hercynian metamorphism are 2–3 kbar and 600 °C; Graessner and Schenk, 1999) and intruded by late-Hercynian peraluminous granites. Alpine metamorphism is concentrated in the lower (northern) part of the Aspromonte Unit (Bonardi et al., 1984a; Platt and Compagnoni, 1990). Two Alpine events have been described; *PT* estimates for the first event are in the range of 5–8 kbar and 480–520 °C (Messina et al., 1992). The second event is limited to meter- to decameter-scale shear zones that clearly postdate the early tectonic stacking (Heymes et al., 2008; see Section 2.3). According to Ortolano et al. (2005) and Cirrincione et al. (2008), *PT* conditions of the retrograde Alpine metamorphic overprint are similar to those of the Africo-Polsi Unit.

Finally, the uppermost unit in the Aspromonte Massif (i.e. the Stilo Unit) corresponds to the parautochthonous upper part of the Aspromonte Unit (Heymes et al., 2008; Fig. 2). It is made up of metamorphics comprising paragneiss, orthogneiss and metamorphosed infra-Paleozoic (?) and Paleozoic sedimentary rocks (Bouillin et al., 1987), unconformably covered by a thin carbonate rich Mesozoic sequence (Roda, 1965; Bonardi et al., 1984b). The Hercynian metamorphic imprint is limited to low greenschist-facies conditions in the southern part of the Stilo Unit, but is progressively stronger northward (i.e., downward, due to the southward tilting of the whole tectonic pile) and reaches amphibolite-facies conditions similar to those of the Aspromonte Unit (Graessner and Schenk, 1999). No Alpine metamorphic overprint has been observed in the Stilo Unit.

2.3. The tectonic evolution of southern Calabria

The Aspromonte Unit extends to the Peloritan Mountains in Sicily, where the units it overlies comprise slices of Mesozoic sedimentary cover (Cirrincione and Pezzino, 1993). The emplacement of the Aspromonte Unit on the Africo-Polsi Unit must be at least in part Alpine, even if De Gregorio et al. (2003) consider that the main stacking phase is Hercynian. Recent structural and metamorphic observations (Heymes et al., 2008) indicate a top-to-SE emplacement direction for the stacking phase in the Aspromonte Massif (Fig. 2), while in the Peloritan Mountains it is rather south-directed (e.g. Somma et al., 2005).

The Stilo and Aspromonte units are separated by a low-angle planar detachment surface. The very clear metamorphic gap (at least in the southern part of the massif) produced by the tectonic superposition of lower grade on higher grade metamorphics indicates that this is an extensional contact (Heymes et al., 2008). The present-day thrust-like geometry of this contact is the result of southward tilting of the whole Aspromonte tectonic pile during Pliocene–Quaternary times (see cross-sections in Fig. 2). Kinematic indicators related to the deformation along this detachment surface confirm a top-to-NE sense of displacement for the Stilo Unit, which corresponds to Alpine extensional reworking of the whole Aspromonte tectonic pile. Extension is also indicated by the reactivation of the basal nappe contact of the Aspromonte Unit with the same kinematic direction (Heymes et al., 2008; Fig. 2). This extensional phase is accompanied by the final exhumation of the lower crustal levels of the massif.

2.4. Available chronological constraints

The oldest available ages in southern Calabria are from the Calabride Complex. U–Pb dating of zircon from orthogneisses yielded Early Cambrian protolith ages (Micheletti et al., 2007). Lower Ordovician ages have been obtained by U–Pb dating of zircon from both felsic and mafic metavolcanics of the Peloritan Mountains (Trombetta et al., 2004). A Hercynian metamorphic imprint of ~295 Ma has been evidenced from U–Pb dating of zircon (Schenk, 1980; Graessner et al., 2000). Ages ranging from 313 Ma to 262 Ma have been obtained for the emplacement of late-Hercynian leucogranites (Rb–Sr on mica, Del Moro et al., 1982; Atzori et al., 1990, and U–Pb on zircon, Graessner et al., 2000; Fiannacca et al., 2008).

In northern Calabria, the Alpine imprint has been dated between 38 and 30 Ma ($^{40}Ar/^{39}Ar$ dating on phengite, Rossetti et al., 2001; Rossetti et al., 2004). These ages are interpreted to reflect the end of high-pressure metamorphism and the onset of extensional tectonics. In southern Calabria, the Alpine metamorphic overprint is poorly dated. Most published geochronological ages are intermediate between Hercynian and Alpine events (see e.g. Rb–Sr dating of Schenk, 1980 and Del Moro et al., 2000) because of the relatively low-temperature conditions prevailing throughout the Alpine evolution. In the Aspromonte Massif, Rb–Sr dating of mica yielded ages ranging between 314 and 22 Ma (Bonardi et al., 1987). There is no precise correlation between these ages and the deformation events described by Bonardi et al. (1992), Platt and Compagnoni (1990) or Heymes et al. (2008). In the Peloritan Mountains, De Gregorio et al. (2003) suggest an age around 301 Ma ($^{40}Ar/^{39}Ar$ dating on white mica) for the nappe stacking phase, but, as mentioned in the previous section, this stacking is at least partly Alpine. In addition we have shown (Heymes et al., 2008) that the extensional reworking of the tectonic pile was initiated before deposition of the post-orogenic Upper Oligocene–Lower Miocene series. And it has been recently confirmed by $^{40}Ar/^{39}Ar$ laser experiments on pseudotachylyte-bearing shear zones yielding an approximate middle Oligocene age for this extensional reworking in southern Calabria (Grande et al., 2009). Finally, available low-temperature thermochronological data (apatite and zircon fission tracks) from southern Calabria show an increase in cooling rate at the Upper Eocene–Lower Oligocene boundary and confirm that exhumation and cooling of the Aspromonte Massif were completed in the Lower Miocene (around 18 Ma; Thomson, 1994).

In order to better constrain the timing of the Alpine tectonometamorphic evolution, we carried out $^{40}Ar/^{39}Ar$ dating on syn-kinematic metamorphic minerals (mainly white micas) of the Aspromonte Massif. In addition, step-heating analyses were performed on K-feldspars in an attempt to precise the age of final exhumation of the basement rocks.

3. Sample description and petrology

The studied samples were collected from the three main tectonic units (see Table 1 for details): (i) the Africo-Polsi Unit (samples TH111, TH140, T157, TH164 and Ca02-113), (ii) the base of the Aspromonte Unit in the shear zone associated to the former thrust surface (samples TH109 and TH269), (iii) near the top of the Aspromonte unit (samples TH013, TH273 and TH276) and (iv) the

Please cite this article as: Heymes, T., et al., Alpine tectonics in the Calabrian–Peloritan belt (southern Italy): New $^{40}Ar/^{39}Ar$ data in the Aspromonte Massif area, Lithos (2009), doi:10.1016/j.lithos.2009.10.011

Table 1
Location and description of studied samples.

Sample	Latitude–longitude	Unit	Lithology	Mineralogy	Separated minerals
Ca02-113	15°46,913 E–38°05,174 N	Africo-Polsi	Micaschist	Qtz-Wm-Chl-Grt	White mica
TH013	15°44,868 E–37°58,336 N	Aspromonte	Orthogneiss	Qtz-Kfs-Pl-Bt	K-Feldspar
TH109	15°59,377 E–38°03,961 N	Aspromonte	Mylonitic gneniss	Qtz-Kfs-Pl-Bt	White mica
TH111	15°59,673 E–38°04,003 N	Africo-Polsi	Micaschist	Qtz-Wm-Chl	White mica
TH140	15°59,339 E–38°09,686 N	Africo-Polsi	Micaschist	Qtz-Wm-Grt-Kfs-Chl	White mica
TH157	15°57,836 E–38°10,128 N	Africo-Polsi	Amphibolitic-schist	Qtz-Amp-Bt-Wm-Grt-Chl	White mica, amphibole
TH164	15°57,710 E–38°09,827 N	Africo-Polsi	Amphibolitic-schist	Qtz-Amp-Bt-Wm-Grt-Chl	White mica, amphibole
TH258	15°52,770 E–38°03,859 N	Stilo	Mylonitic gneiss	Qtz-Kfs-Pl-Wm	White mica
TH269	15°57,830 E–38°10,570 N	Aspromonte	Mylonitic gneiss	Qtz-Kfs-Pl-Wm	White mica
TH273	15°59,624 E–37°55,540 N	Aspromonte	Paragneiss	Qtz-Kfs-Pl-Bt	K-feldspar
TH276	15°00,609 E–37°55,650 N	Aspromonte	Paragneiss	Qtz-Kfs-Pl-Bt	K-feldspar

Qtz: quartz; Wm: white mica; Chl: chlorite; Grt: garnet; Amp: amphibole; Pl: plagioclase; Kfs: feldspar; Bt: biotite.

base of the Stilo Unit near the uppermost detachment surface (sample TH258) (Fig. 2).

3.1. Africo-Polsi Unit

In this unit our principal objective was to date the main metamorphic steps that predated the extensional tectonic phase. All samples have been collected a few meters to decameters below the tectonic top of the unit. Three samples (TH140, TH157 and TH164) derive from the lowermost (northern) part of the unit, where the Alpine metamorphic overprint is strongest. The other two samples were collected from relatively shallower levels, in the western (Ca02-113) and southern parts of the unit (TH111). For all samples we extracted bulk separates of white mica. In addition, two bulk separates of amphibole were extracted from samples TH157 and TH164.

Sample Ca02-113 is a garnet-bearing micaschist from the Cardeto area in the western part of the Aspromonte Massif. White mica lies in the main foliation together with quartz and chlorite (Fig. 3). This foliation surrounds often fragmented large (size >1 mm) garnet porphyroclasts. The dated white micas have a Si content (p.f.u.) ranging from 3.04 to 3.23 (Table 2, Fig. 4) suggesting that these minerals are probably relatively low-pressure white micas (Massonne and Schreyer, 1987). In addition, the significant Na_2O content indicates probable paragonite interlayers.

The other samples from the Africo-Polsi Unit were collected in the main tectonic window on the Ionian side of the massif (Fig. 2). Sample TH140 is a very light-colored garnet-bearing micaschist. The foliation is composed of quartz, white mica, idioblastic garnet and rare biotite and plagioclase. Secondary chlorite occurs in some pressure shadows of millimeter-sized garnet porphyroclasts. The dated white micas have a Si content (p.f.u.) ranging from 3.14 to 3.34 (Table 2, Fig. 4) and SEM images (Fig. 5a) illustrate the complex intergrowths of successive generations of white mica. The higher Si content is probably indicative of higher pressure conditions (Massonne and Schreyer, 1987) in this part of the Africo-Polsi Unit compared to its western part (sample Ca02-113). Samples TH157 and TH164 are blue–green amphibole-bearing schists. The foliation displays a quartz, biotite, white mica, chlorite and idioblastic garnet paragenesis (Fig. 3). Large relict porphyroclasts of garnet, sub-rounded blue–green amphibole and large white micas, wrapped around by the main foliation, probably belong to an older paragenesis. The blue–green amphiboles show a variable chemical composition (Table 2, Fig. 4): in sample TH157, their composition is homogeneous, while in sample TH164 they range from tschermakitic hornblende to pargasite compositions.

In sample TH111, collected from the southern area of the Africo-Polsi Unit, evidence for a relatively high-temperature older paragenesis is lacking. Most probably, Hercynian metamorphism did not exceed greenschist facies in that area. The foliation is defined by an assemblage of quartz, chlorite, white mica, epidote and rare biotite (Fig. 3). The dated white micas show a relatively homogeneous composition with a Si content (p.f.u.) ranging from 3.16 to 3.20 but it is likely that there are grains from different generations as suggested by the complex textural relationships observed on SEM images (Fig. 5b).

All samples were affected by discrete shear planes showing late recrystallization of quartz, chlorite and white mica in the northern part (samples Ca02-113, TH140, TH157 and TH164) and very fine-grained white mica, quartz and chlorite in the southern part (sample TH111) of the unit. These recrystallizations are clearly related to the NE-directed Alpine extensional reworking phase (Platt and Compagnoni, 1990; Heymes et al., 2008), while the main foliation was probably acquired during the stacking phase. White micas from these shear planes exhibit a similar chemical composition as those from the main foliation but it is likely that the white mica bulk separate consists of several generations. As it will be illustrated in Section 4.2, this coexistence of multiple generations of white mica generally gives rise to complex $^{40}Ar/^{39}Ar$ geochronological results (e.g. Wijbrans and McDougall, 1986; Monié, 1990; Dunlap, 1997).

3.2. Aspromonte Unit

3.2.1. Lower tectonic contact of Aspromonte Unit

Samples TH109 and TH269 are mylonitic gneisses collected from the basal shear contact of the Aspromonte Unit, respectively in the southern and northern parts of the main tectonic window (Fig. 2). To date the movement along this major tectonic contact, bulk separates of white mica were extracted from these two samples.

Both samples display mylonitic deformation, which transposes an older foliation and which seems to increase in intensity northward. In sample TH109, the mylonitic fabric is mainly cataclastic and marked by weak quartz recrystallization and fracturing of feldspar, while in sample TH269, the mylonitic recrystallization is marked by very thin quartz and white mica ribbons wrapping around sub-rounded feldspar porphyroclasts (Fig. 3). Despite the complex tectonic history (the contact acted initially as a thrust and then as a detachment), white micas from sample TH269 show a relatively homogeneous chemical composition with a Si content (p.f.u.) ranging from 3.14 to 3.17 (Table 2, Fig. 4).

3.2.2. Upper part of Aspromonte Unit

Three other samples (TH013, TH273 and TH276) were collected from the topmost part of the Aspromonte Unit, only a few meters below the contact with the Stilo Unit (Fig. 2). For the three samples bulk separates of K-feldspar were extracted in order to recover the cooling age related to the exhumation of the Aspromonte Unit.

Sample TH013 is an orthogneiss collected from the western part of the massif in a kilometer-wide tectonic window. In this area, deformation and recrystallization associated with extensional tectonics are limited to a meter-thick shear zone. Sample TH013 has been collected about 2 m below the top of the Aspromonte Unit. Samples

Please cite this article as: Heymes, T., et al., Alpine tectonics in the Calabrian–Peloritan belt (southern Italy): New $^{40}Ar/^{39}Ar$ data in the Aspromonte Massif area, Lithos (2009), doi:10.1016/j.lithos.2009.10.011

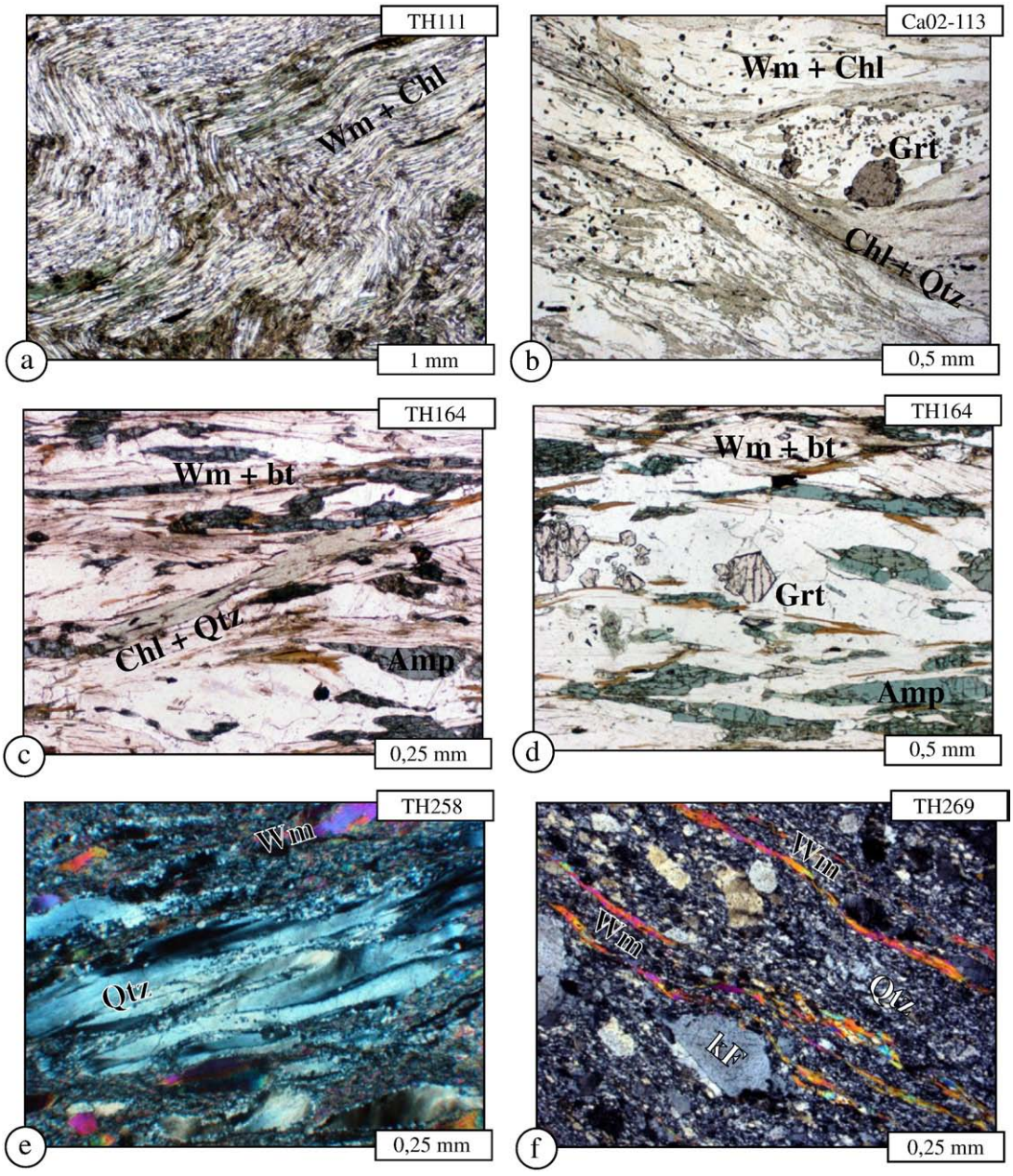

Fig. 3. Thin section microphotographs showing representative metamorphic parageneses and microstructures of selected samples. (a–d) Micaschists and amphibole-bearing schists from the Africo-Polsi Unit (plane polarized light). (e–f) Mylonitic gneisses (crossed polarizers) from shear zones at the base to the Stilo Unit (close to the upper detachment surface) and at the base of the Aspromonte Unit (reworked thrust contact) respectively. For sample locations see Fig. 2. Wm: white mica; Chl: chlorite; Bt: biotite; Amp: amphibole; Grt: garnet; Qtz: quartz; kF: K-feldspar.

TH273 and TH276 are paragneisses collected from the southernmost part of the massif (Fig. 2), where the Stilo Unit consists of only a few tens of meters of slightly metamorphic schists and carbonates covered by non-metamorphic Mesozoic carbonates. In that area, a sharp lithological and metamorphic contrast between the Aspromonte and the Stilo units is evident, and makes the detachment contact very obvious. Both hanging wall and footwall rocks are locally brecciated but samples TH273 and TH276 have been collected outside the brecciated zones.

3.3. Stilo Unit

Sample TH258 was collected from the base of the Stilo Unit, within the extensional shear zone separating the Stilo and the Aspromonte units. It derives from the deepest exposed part of the detachment, where this low-angle fault cuts the late-Hercynian Punta d'Atò granitic intrusion (Fig. 2). This sample, a light-colored mylonitic gneiss (Fig. 3), has been collected to date the detachment and the time at which the Aspromonte and the Stilo Units tectonically divided. The white micas separated from this sample are magmatic muscovite porphyroclasts partially recrystallized during mylonitization.

4. $^{40}Ar/^{39}Ar$ dating

4.1. Analytical procedure

Two techniques for argon extraction have been used during this $^{40}Ar/^{39}Ar$ geochronological study. Most analyses were carried out on bulk separates of white mica, amphibole and K-feldspar using step-wise heating procedure in a furnace. In addition, single crystals of white mica were extracted from samples TH164 and TH258 and progressively degassed using a laser probe. Minerals separated from

Please cite this article as: Heymes, T., et al., Alpine tectonics in the Calabrian–Peloritan belt (southern Italy): New $^{40}Ar/^{39}Ar$ data in the Aspromonte Massif area, Lithos (2009), doi:10.1016/j.lithos.2009.10.011

Table 2
Representative electron microprobe analyses of dated white micas and amphiboles.

Sample	Ca02-113		TH111		TH140		TH157		TH164		TH269		TH157		TH164	
Unit	APU		APU		APU		APU		APU		AU		APU		APU	
Mineral	Wm		Wm		Wm		Wm		Wm		Wm		Wm		Wm	
SiO_2	45.855	46.704	46.17	46.066	46.118	48.501	45.373	46.562	46.764	47.592	46.176	47.056	43.652	42.327	44.612	41.883
TiO_2	0.389	0.000	0.515	0.588	0.476	0.699	0.788	0.686	0.770	0.656	0.132	0.000	0.000	0.557	0.449	0.532
Al_2O_3	34.053	31.045	30.245	29.642	32.762	29.022	29.957	28.555	31.418	29.763	33.009	33.904	13.677	14.431	13.967	14.395
FeO	1.603	2.103	3.661	3.332	1.681	1.292	2.483	2.123	2.874	2.928	1.114	1.147	15.162	15.404	17.493	17.521
MnO	0.000	0.000	0.000	0.000	0.000	0.000	0.000	0.000	0.000	0.000	0.122	0.095	0.000	0.000	0.000	0.000
MgO	0.844	1.651	2.494	1.813	1.283	2.312	1.997	2.453	1.775	2.225	1.250	1.213	10.025	9.414	9.304	8.503
CaO	0.000	0.000	0.000	0.000	0.000	0.000	0.000	0.000	0.000	0.000	0.019	0.057	10.667	11.081	9.421	10.388
Na_2O	1.542	1.216	0.561	0.511	1.269	1.454	0.821	0.699	1.114	0.768	0.289	0.178	2.223	2.316	2.319	2.942
K_2O	9.026	9.592	10.238	10.253	9.824	9.234	10.053	10.065	10.162	10.393	11.032	10.045	0.446	0.269	0.337	0.461
Total	93.312	92.311	93.882	92.203	93.413	92.511	91.468	91.142	94.877	94.325	93.146	93.698	95.852	95.794	97.902	96.623
Structural formula																
Si	3.107	3.215	3.165	3.208	3.137	3.310	3.176	3.259	3.159	3.233	3.152	3.165	6.563	6.396	6.592	6.353
Al	2.719	2.518	2.443	2.432	2.626	2.334	2.471	2.355	2.501	2.382	2.655	2.687	2.423	2.570	2.432	2.573
Ti	0.019	0.000	0.026	0.030	0.024	0.035	0.041	0.036	0.039	0.033	0.006	0.000	0.000	0.063	0.049	0.060
Fe^{2+}	0.090	0.121	0.209	0.194	0.095	0.073	0.145	0.124	0.162	0.166	0.063	0.064	1.906	1.946	2.161	2.222
Mn	0.000	0.000	0.000	0.000	0.000	0.000	0.000	0.000	0.000	0.000	0.007	0.005	0.000	0.000	0.000	0.000
Mg	0.085	0.169	0.254	0.188	0.130	0.235	0.208	0.255	0.178	0.225	0.127	0.121	2.246	2.119	2.049	1.922
Ca	0.000	0.000	0.000	0.000	0.000	0.000	0.000	0.000	0.000	0.000	0.001	0.004	1.718	1.794	1.491	1.688
Na	0.202	0.162	0.074	0.068	0.167	0.192	0.111	0.094	0.145	0.101	0.038	0.023	0.648	0.678	0.664	0.865
K	0.779	0.842	0.895	0.910	0.852	0.803	0.897	0.898	0.875	0.900	0.960	0.861	0.085	0.051	0.063	0.089
Sum.	7.004	7.027	7.070	7.033	7.034	6.984	7.050	7.023	7.061	7.042	7.012	6.933	15.591	15.620	15.505	15.776

APU: Africo-Polsi Unit; AU: Aspromonte Unit; Wm: white mica; Amp: amphibole.

these two samples were hand-picked under a binocular microscope directly on the rock sample or from the 1000–500 µm fraction after crushing and sieving. According to textural relationships, these large grains are porphyroclasts of probable Hercynian age that experienced partial recrystallization in Alpine times. Bulk separates of white mica, amphibole and K-feldspar from all other samples (including white

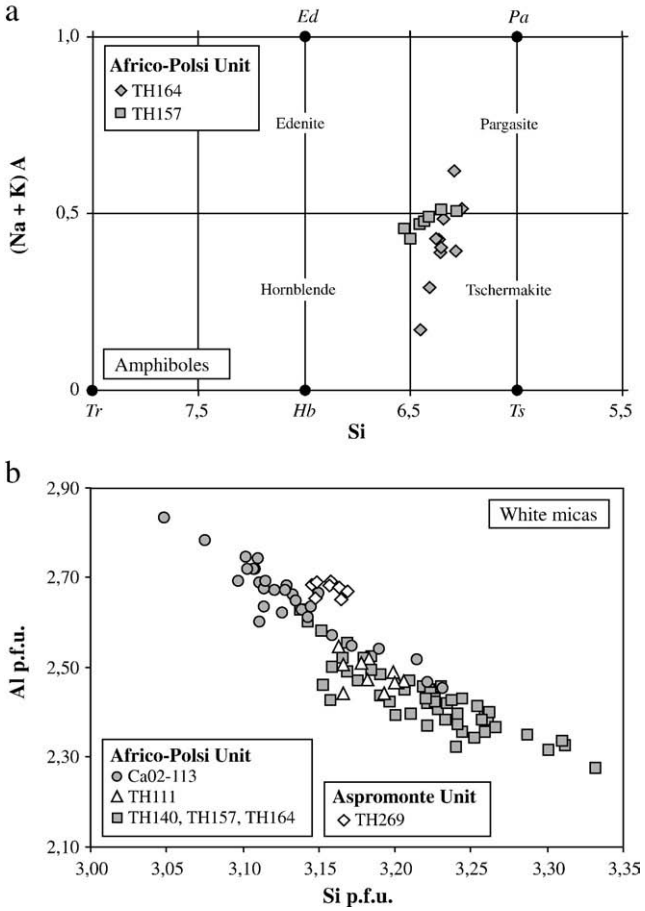

Fig. 4. (a) Si versus (Na + K) diagram for amphiboles (classification after Leake et al., 2004) and (b) Si versus Al diagram for white micas (electron microprobe acquisition beam current parameters: 15 kV, 20 nA). See Table 2 for details.

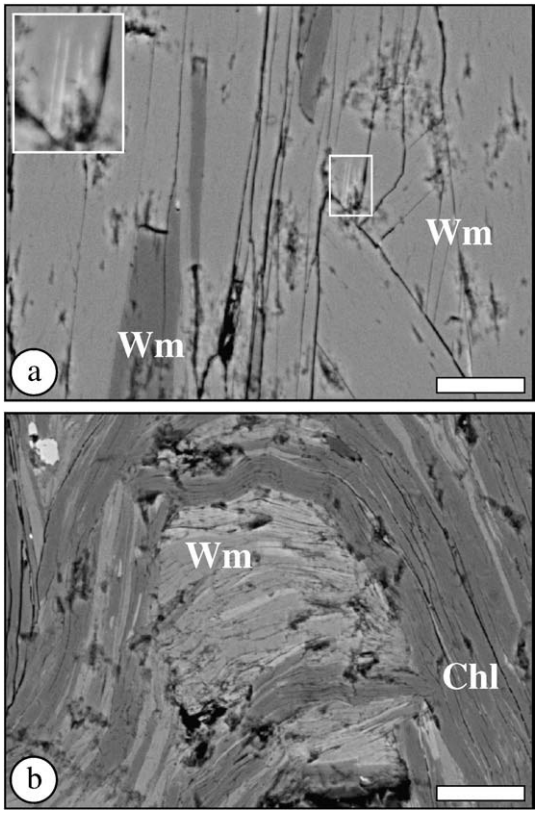

Fig. 5. BSE images of two selected samples from the Africo-Polsi Unit: (a) coarse-grained white mica in sample TH140 from the lower part of the unit; (b) very fine-grained chlorite and white mica in sample TH111 from the upper part of the unit. The complex overgrowths within the white mica are illustrated by the different patches of grey. Scale bar: 20 µm.

Please cite this article as: Heymes, T., et al., Alpine tectonics in the Calabrian–Peloritan belt (southern Italy): New $^{40}Ar/^{39}Ar$ data in the Aspromonte Massif area, Lithos (2009), doi:10.1016/j.lithos.2009.10.011

micas of sample TH164 also used for single-grain dating) were extracted from the 125–160 μm fraction using classical magnetic and density separation techniques. After acetone, alcohol and distilled water washing, samples were loaded in Aluminium packets and irradiated in the 5c position of the McMaster nuclear reactor (Canada) together with several aliquots of MMHb and Fish Canyon Sanidine flux monitors (Samson and Alexander, 1987; Lanphere and Baadsgaard, 2001, Jourdan and Renne, 2007). The samples were irradiated in several batches. The effects of interfering reactions with Ca and K were evaluated using the following correction factors obtained during a previous irradiation (see also McDougall and Harrison, 1999): $(^{40}Ar/^{39}Ar)_K = 0.0156$; $(^{39}Ar/^{37}Ar)_{Ca} = 0.000651$; $(^{36}Ar/^{37}Ar)_{Ca} = 0.000254$.

Single crystals were degassed by means of a defocused continuous 50 W CO_2 laser with a beam diameter at least twice the size of the heated grain. After heating and gas cleaning, argon was introduced in a MAP 215-250 mass spectrometer with a Nier ion source and a Johnston MM1 electron multiplier. Each analysis involved 5 min for gas extraction and cleaning and 8 min for data acquisition by peak switching from argon mass 40 to 36. Isotopic compositions were estimated by regression on 12 to 15 runs. System blanks were evaluated every three experiments. They were in the range of 2×10^{-12} cm^3 for ^{40}Ar, 1.5×10^{-14} cm^3 for ^{39}Ar, 3×10^{-15} cm^3 for ^{38}Ar, 6×10^{-14} cm^3 for ^{37}Ar and 7×10^{-15} cm^3 for ^{36}Ar. Populations of white mica, amphibole and K-feldspar were loaded into a double vacuum Staudacher-type furnace, the temperature of which was calibrated by means of a thermocouple placed at the base of the crucible. Each step included 20 min of heating and 5 min of cleaning on Al–Zr getters and cold traps and 12 min of measurement on a VG3600 mass spectrometer. Signals were collected on a Faraday cup for ^{40}Ar and ^{39}Ar, while ^{39}Ar, ^{38}Ar, ^{37}Ar and ^{36}Ar were analyzed with a photomultiplier after interaction on a Daly plate. Details for each analysis are reported in Table 3. A particular step-heating schedule was conducted on K-feldspar bulk separates in an attempt to identify excess argon from possible fluid inclusions. We thus conducted duplicated isothermal step heating at low temperatures (450–800 °C), often yielding a sawtooth-shaped age spectrum where the second of the two stages is systematically younger and probably less affected by excess argon (e.g. Harrison et al., 1994).

For all analyses, mass discrimination was calculated on the basis of an $^{40}Ar/^{36}Ar$ ratio of 292.0 ± 1.7 for the VG3600 mass spectrometer and 289.0 ± 2.1 for the MAP 215-50 mass spectrometer. For each individual age reported in Table 4, usual isotope corrections including blanks, mass discrimination, radioactive decay of ^{37}Ar and ^{39}Ar and irradiation-induced mass interference were applied. Errors reported for individual steps take into account the errors introduced by these corrections as well as the analytical errors on signals. The uncertainty on the *J*-factor was propagated in the calculation of the error on the total age of each sample, equivalent to a K–Ar age.

A "plateau age" is defined as the portion of a spectrum, made of three consecutive steps, comprising more than 70% of the total ^{39}Ar released, and whose ages overlap within two sigma errors (e.g. McDougall and Harrison, 1999). However, due to the polycyclic evolution of the Calabria basement rocks, such criteria were not satisfied by many age spectra. In these cases, a pseudo-plateau age was proposed for which the following alternative definitions have been adopted: 1) it includes two or more consecutive steps containing more than 50% of the total amount of ^{39}Ar released with apparent ages reproducible at the 90% confidence level; 2) it includes steps containing less than 50% of the total amount of ^{39}Ar released with apparent ages reproducible at the 95% confidence interval. For Ca- or Cl-bearing samples, K/Ca and Cl/K plots can be derived from $^{39}Ar/^{37}Ar$ and $^{38}Ar/^{39}Ar$ ratios used as a proxy for the true elemental ratios. Isochron ages, when reliable, were calculated in an inverse isochron diagram of $^{36}Ar/^{40}Ar$ versus $^{39}Ar/^{40}Ar$, following the regression technique of York (1969). The quality of the linear fit relative to individual errors is measured with the mean square weighted deviation (MSWD). All ages are given at the one standard deviation (1σ) confidence level. For each sample, the preferred age is highlighted in Table 4.

4.2. $^{40}Ar/^{39}Ar$ results

All the age spectra obtained show a disturbed pattern, with saddle, staircase or more complex shapes (Fig. 6). These variable patterns can result from: (i) temperature induced argon diffusion (Turner, 1971), (ii) deformation induced partial recrystallization (Scheuber et al., 1995; Dunlap, 1997; Heizler et al., 1997; Worley et al., 1997; Villa, 1998); (iii) mixture of mineral generations (Wijbrans and McDougall, 1986; Villa et al., 1997), (iv) complex mineralogical systems (e.g. perthitic feldspars, Parsons and Brown, 1988), (v) fluid-induced retrogression and fluid-assisted recrystallization (Villa, 1998; Alexandrov et al., 2002), (vi) excess argon (e.g. Harrison and McDougall, 1981; Li et al., 1994; Arnaud and Kelley, 1995) or a combination of several of these possible effects.

4.2.1. Africo-Polsi Unit

4.2.1.1. Amphiboles. Amphiboles of samples TH157 and TH164 yielded very disturbed age spectra with no plateau portion. For sample TH157 (Fig. 6a) ages range between a minimum of 83.3 ± 1.5 Ma and a maximum of 450 ± 15 Ma for a total fusion age calculated at 147 ± 0.9 Ma. Excess argon was released during the first heating increments, then ages progressively increased from a minimum of 83 Ma to a maximum of 162 Ma. The correlative variation of K/Ca and Cl/K ratios confirms the complex composition of the analysed population of amphiboles, already suggested by our chemical analyses. This isotopic and chemical heterogeneity is also supported by the non-linear distribution of data in the inverse isochron diagram. Similar observations can be made for the age spectrum of sample TH164 (Fig. 6b). Ages range between a minimum of 62.7 ± 2.6 Ma and a maximum of 288 ± 2.5 Ma for a total fusion age of 145 ± 1.6 Ma. The discordant K/Ca and Cl/K patterns and the strong scattering of representative data points in the $^{36}Ar/^{40}Ar$ versus $^{39}Ar/^{40}Ar$ isotope diagram suggest that different reservoirs contributed to the gas released. No meaningful data can thus be obtained from these amphiboles with ages intermediate between the Hercynian and Alpine orogenic events.

4.2.1.2. White micas. In the southern part of the Africo-Polsi Unit, white mica bulk separate from sample TH111 yielded a staircase-shaped spectrum that progressively increases from a minimum age of 45.9 ± 8.2 Ma to a maximum age of 326 ± 0.8 Ma, for a total fusion age of 255 ± 2.4 Ma (Fig. 6c). These variations are anti-correlated with Cl/K ratios, while the Ca/K plot suggests that the dated bulk separate was compositionally heterogeneous. Such chemical and age heterogeneity is not clearly supported by the microprobe analyses (Fig. 4), which suggest that a single mica type defines the foliation. This could mean that Alpine and pre-Alpine minerals have nearly the same composition in this sample, or that our microprobe analyses are not representative of pre-Alpine minerals. As illustrated by the SEM imagery (Fig. 5b), we cannot exclude the presence of partly preserved older minerals in this very fine-grained rock. No clear linear trend appears in the $^{36}Ar/^{40}Ar$ versus $^{39}Ar/^{40}Ar$ isotope diagram. It is likely that the minimum age of 46 Ma represents a maximum age limit for the Alpine overprint and 326 Ma a minimum age limit for the Hercynian metamorphism.

In contrast, white mica bulk separates from samples TH140, TH157 and TH164 from a deeper part of the Africo-Polsi Unit yielded partially concordant age spectra for which Alpine pseudo-plateau ages have been calculated (Fig. 6). For sample TH140, step heating ages range from a minimum of 23.7 ± 0.5 Ma to a maximum of 34.2 ± 0.3 Ma. The total fusion age (32.3 ± 0.1 Ma) is very close to the pseudo-plateau age of 33.0 ± 0.3 Ma defined by three successive steps (5 to 7) corresponding to 77% of the total argon released (Fig. 6d). The absence

Please cite this article as: Heymes, T., et al., Alpine tectonics in the Calabrian–Peloritan belt (southern Italy): New $^{40}Ar/^{39}Ar$ data in the Aspromonte Massif area, Lithos (2009), doi:10.1016/j.lithos.2009.10.011

Table 3
$^{40}Ar/^{39}Ar$ data.

Step	$^{40}Ar/^{39}Ar$	$^{38}Ar/^{39}Ar$	$^{37}Ar/^{39}Ar$	$^{36}Ar/^{39}Ar$ (E−3)	^{39}Ar (E−14)	%^{39}Ar	%$^{40}Ar^{*}$	$^{40}Ar^{*}/^{39}K$	Age (Ma)	Error
TH157_Amp										
$J=0.009091$										
600	488.231	0.776	4.69945	1638.604	0.018	0.18	0.88	4.3	69.199	484.82
700	251.382	0.39	3.86574	794.489	0.019	0.38	6.69	16.87	257.373	193.18
800	54.109	0.099	2.73471	78.245	0.056	0.95	57.54	31.19	450.331	15.737
850	17.805	0.075	0.76741	20.572	0.123	2.19	66.01	11.76	183.225	1.77
900	29.814	0.069	0.42705	80.339	0.239	4.62	20.39	6.08	97.074	2.233
950	19.336	0.066	0.5934	41.121	0.169	6.34	37.24	7.2	114.439	2.671
1000	16.851	0.076	0.90782	27.234	0.264	9.02	52.45	8.84	139.506	1.87
1050	7.333	0.127	2.81354	7.769	0.762	16.76	70.74	5.2	83.292	1.573
1100	10.223	0.271	5.99319	8.151	1.138	28.28	79.8	8.19	129.554	0.476
1200	9.842	0.311	0	0	5.284	82.02	99.8	9.82	154.303	0.107
1400	16.422	0.323	8.13595	22.361	1.777	100	62.64	10.34	162.102	0.499
TH164_Amp										
$J=0.008888$										
500	24.146	0.181	0.36125	51.800	0.092	6.61	36.61	8.84	136.493	10.587
600	14.059	0.086	0.08972	34.053	0.073	11.86	28.32	3.98	62.747	2.636
650	13.233	0.103	0.11541	13.024	0.055	15.80	70.82	9.37	144.343	3.862
700	11.369	0.106	0.15597	9.811	0.062	20.27	74.41	8.46	130.796	1.603
750	9.251	0.104	0.28217	0.613	0.069	25.23	98.01	9.07	139.847	0.790
800	7.445	0.128	0.39442	5.765	0.090	31.70	77.17	5.75	89.879	5.234
850	7.108	0.162	0.51270	7.548	0.112	39.77	68.77	4.89	76.751	4.552
900	12.245	0.283	1.39776	4.231	0.360	65.61	90.32	11.07	169.296	2.887
950	9.487	0.201	1.37227	10.351	0.184	78.80	68.42	6.50	101.275	6.891
1000	9.838	0.184	1.82410	7.851	0.089	85.20	77.34	7.62	118.185	6.430
1050	17.645	0.237	1.89652	9.794	0.047	88.61	84.14	14.86	223.866	2.914
1100	24.135	0.318	1.89462	24.424	0.028	90.62	70.49	17.03	254.325	21.889
1200	24.174	0.319	1.83112	16.245	0.075	96.02	80.52	19.49	288.178	2.515
1400	25.829	0.322	1.81837	36.936	0.055	100.00	58.09	15.02	226.093	8.874
TH111_Wm										
$J=0.009091$										
600	50.108	0.263	0.00005	86.792	0.01	0.07	48.78	24.44	361.984	18.419
700	22.641	0.109	0.30227	67.017	0.024	0.24	12.52	2.84	45.926	8.188
800	9.44	0.029	0.0713	6.115	0.243	1.96	80.69	7.62	120.805	0.785
850	9.268	0.017	0.11809	1.256	0.379	4.63	95.86	8.89	140.136	0.379
900	12.675	0.018	0.01496	10.361	0.942	11.29	75.69	9.59	150.872	0.591
950	13.935	0.013	0.00244	0.976	2.28	27.39	97.79	13.63	210.697	0.344
1000	17.364	0.013	0.00121	0.467	4.102	56.36	99.09	17.21	262.187	0.258
1050	19.067	0.013	0.00344	0.587	3.964	84.36	98.99	18.87	285.687	0.264
1100	20.052	0.013	0.01277	0.847	1.74	96.65	98.66	19.78	298.369	0.412
1200	23.209	0.014	0.08544	4.622	0.414	99.57	94.05	21.83	326.599	0.853
1400	90.503	0.096	0.15032	201.512	0.061	100	34.19	30.95	447.256	12.837
TH140_Wm										
$J=0.009091$										
600	31.018	0.238	0.22965	111.49	0.019	0.09	−6.23	−1.93	0	0
700	11.904	0.078	0.17195	24.877	0.044	0.3	38.16	4.54	73.018	5.314
800	3.766	0.026	0.0172	7.444	0.275	1.58	41.08	1.55	25.198	0.952
850	2.966	0.02	0.01838	3.009	0.496	3.9	69.38	2.06	33.442	0.494
900	5.426	0.02	0.00712	13.369	0.967	8.43	26.83	1.46	23.718	0.492
950	2.428	0.014	0.0015	1.77	2.099	18.25	77.65	1.89	30.661	0.154
1000	2.275	0.011	0.00032	0.503	6.563	48.98	92.59	2.11	34.227	0.287
1050	2.291	0.014	0.00126	0.841	7.262	82.98	88.29	2.02	32.878	0.071
1100	2.131	0.013	0.00204	0.266	2.726	95.75	95.38	2.03	33.037	0.08
1200	2.517	0.015	0.01961	2.787	0.804	99.51	66.53	1.67	27.257	0.309
TH157_Wm										
$J=0.009091$										
600	55.488	0.177	0.00005	129.287	0.012	0.06	31.11	17.26	262.998	33.025
700	20.523	0.108	0.0916	60.744	0.03	0.22	12.47	2.56	41.488	10.713
800	4.649	0.03	0.0342	9.784	0.222	1.39	37.43	1.74	28.318	1.147
850	4.099	0.019	0.01132	3.731	0.456	3.79	72.63	2.98	48.184	0.838
900	6.459	0.025	0.01281	13.62	0.908	8.56	37.4	2.42	39.189	0.799
950	2.473	0.015	0.00329	0.703	1.749	17.77	90.8	2.25	36.461	0.167
1000	2.216	0.014	0.00151	0.698	5.588	47.18	89.79	1.99	32.339	0.085
1050	2.26	0.014	0.00431	0.822	5.86	78.03	88.38	2	32.465	0.159
1100	2.281	0.014	0.01036	0.671	2.969	93.66	90.46	2.06	33.527	0.083

(continued on next page)

Please cite this article as: Heymes, T., et al., Alpine tectonics in the Calabrian–Peloritan belt (southern Italy): New $^{40}Ar/^{39}Ar$ data in the Aspromonte Massif area, Lithos (2009), doi:10.1016/j.lithos.2009.10.011

Table 3 (*continued*)

Step	$^{40}Ar/^{39}Ar$	$^{38}Ar/^{39}Ar$	$^{37}Ar/^{39}Ar$	$^{36}Ar/^{39}Ar$ (E−3)	^{39}Ar (E−14)	$\%^{39}Ar$	$\%^{40}Ar^*$	$^{40}Ar^*/^{39}K$	Age (Ma)	Error
TH157_Wm										
$J=0.009091$										
1200	2.555	0.013	0.00782	1.394	1.064	99.26	83.12	2.12	34.503	0.188
1400	46.134	0.04	0.07061	155.061	0.141	100	0.65	0.3	4.875	6.113
TH164_Wm1										
$J=0.008888$										
500	4.324	0.023	0.11403	7.717	0.611	3.21	46.96	2.03	32.273	0.440
600	2.837	0.016	0.01690	2.312	0.896	7.91	75.24	2.13	33.903	0.224
650	2.812	0.014	0.01024	2.279	1.065	13.50	75.36	2.12	33.658	0.238
700	2.570	0.014	0.00497	1.695	2.340	25.79	79.75	2.05	32.563	0.078
750	2.341	0.014	0.00289	0.974	3.177	42.47	86.86	2.03	32.310	0.108
800	2.397	0.014	0.00579	1.148	2.794	57.14	85.03	2.04	32.388	0.104
850	2.493	0.014	0.00667	1.359	2.558	70.57	83.11	2.07	32.923	0.094
900	2.436	0.014	0.00596	1.046	2.603	84.23	86.50	2.11	33.478	0.096
950	2.324	0.014	0.00683	0.601	2.030	94.89	91.51	2.13	33.787	0.120
1000	2.641	0.014	0.02035	0.049	0.636	98.23	98.75	2.61	41.346	0.146
1050	3.601	0.013	0.05295	2.413	0.229	99.43	79.73	2.87	45.459	4.959
1100	6.764	0.002	0.00002	0.002	0.066	99.78	99.70	6.74	105.013	1.237
1200	17.096	0.000	0.00004	17.776	0.027	99.92	69.16	11.82	180.270	17.071
TH164_Wm2										
$J=0.008888$										
1	3.164	0.016	0.00038	0.000	4.426	14.58	99.37	3.14	49.720	1.393
2	2.436	0.013	0.00000	1.070	6.505	36.00	86.20	2.10	33.362	0.639
3	3.402	0.018	0.02489	3.786	2.085	42.87	66.57	2.27	35.959	1.899
4	2.937	0.027	0.00000	4.574	0.825	45.59	53.30	1.57	24.926	4.848
5	3.851	0.015	0.06270	5.195	3.140	55.93	59.72	2.30	36.511	1.414
6	5.458	0.028	0.00000	11.108	0.843	58.71	39.50	2.16	34.240	5.092
7	8.568	0.016	0.00000	5.723	4.057	72.08	80.03	6.86	106.727	1.439
8	8.732	0.022	0.00000	3.476	8.477	100.00	88.01	7.69	119.204	0.927
Ca02-113_Wm										
$J=0.008628$										
600	159.162	0.515	0.42520	474.583	0.003	0.01	11.89	18.93	272.979	125.17
700	22.874	0.059	0.04045	61.559	0.051	0.19	20.40	4.67	71.197	5.552
750	8.803	0.025	0.03931	20.892	0.087	0.50	29.67	2.61	40.203	2.405
800	4.840	0.019	0.00250	5.855	0.182	1.15	63.85	3.09	47.471	1.213
850	4.473	0.019	0.00762	6.887	0.368	2.46	54.07	2.42	37.258	0.588
900	3.961	0.017	0.00475	3.831	0.960	5.88	70.92	2.81	43.202	0.278
950	2.990	0.014	0.00285	1.245	1.587	11.54	87.04	2.60	40.066	0.230
1000	2.591	0.011	0.00030	0.584	6.706	35.42	92.57	2.40	36.950	0.075
1050	2.459	0.011	0.00087	0.401	7.717	62.91	94.37	2.32	35.769	0.057
1100	2.435	0.011	0.00045	0.217	9.189	95.64	96.54	2.35	36.221	0.054
1200	3.096	0.013	0.00545	0.760	1.128	99.66	92.11	2.85	43.852	0.109
1400	47.940	0.041	0.00000	124.904	0.097	100.00	22.97	11.01	163.732	3.173
TH109_Wm										
$J=0.009091$										
600	15.694	0.064	0.02309	44.102	0.096	0.26	16.84	2.64	42.845	3.754
700	13.510	0.000	0.13770	23.966	0.034	0.34	47.49	6.42	102.289	7.182
800	6.441	0.020	0.01383	8.057	0.375	1.34	62.74	4.04	65.097	0.672
850	5.608	0.015	0.01041	3.331	0.679	3.14	82.10	4.60	73.976	0.398
900	6.714	0.016	0.00482	5.441	1.590	7.35	75.76	5.09	81.560	0.260
950	6.625	0.014	0.00236	1.010	2.464	13.88	95.19	6.31	100.578	0.243
1000	8.550	0.013	0.00121	1.355	6.112	30.08	95.08	8.13	128.641	0.163
1050	9.780	0.014	0.00181	0.836	9.038	54.04	97.27	9.51	149.641	0.118
1100	9.770	0.014	0.00194	0.831	10.448	81.73	97.28	9.50	149.519	0.111
1200	10.090	0.013	0.00569	0.762	6.428	98.77	97.57	9.84	154.643	0.128
1400	17.810	0.024	0.02635	26.801	0.465	100.00	55.43	9.87	155.049	1.086
TH269_Wm1										
$J=0.009091$										
600	110.138	0.558	0.10479	167.249	0.003	0.05	55.11	60.71	792.838	240.10
700	14.905	0.053	0.00002	59.566	0.026	0.4	−18.23	−2.72	0	0
800	4.917	0	0.0146	5.134	0.075	1.44	68.75	3.38	54.61	1.081
850	3.537	0.008	0.02526	5.649	0.141	3.38	52.28	1.85	30.077	1.157
900	9.341	0.021	0.02249	29.746	0.484	10.05	5.7	0.53	8.714	0.616
950	2.056	0.013	0.00275	0.933	1.75	34.15	85.63	1.76	28.641	0.142
1000	1.96	0.013	0.00185	0.647	2.128	63.46	89.23	1.75	28.454	0.096

Please cite this article as: Heymes, T., et al., Alpine tectonics in the Calabrian–Peloritan belt (southern Italy): New $^{40}Ar/^{39}Ar$ data in the Aspromonte Massif area, Lithos (2009), doi:10.1016/j.lithos.2009.10.011

Table 3 (*continued*)

Step	$^{40}Ar/^{39}Ar$	$^{38}Ar/^{39}Ar$	$^{37}Ar/^{39}Ar$	$^{36}Ar/^{39}Ar$ (E−3)	^{39}Ar (E−14)	%^{39}Ar	%$^{40}Ar^{*}$	$^{40}Ar^{*}/^{39}K$	Age (Ma)	Error
TH269_Wm1										
$J=0.009091$										
1050	1.947	0.013	0.00454	0.922	1.709	86.99	85	1.65	26.934	0.129
1100	2.075	0.013	0.01702	2.264	0.804	98.06	66.85	1.39	22.612	0.258
1200	7.06	0.015	0.11791	28.053	0.093	99.33	−17.6	−1.24	0	0
1400	159.337	0.135	0.0904	572.475	0.048	100	−6.18	−9.84	0	0
TH269_Wm2										
$J=0.009065$										
750	7.451	0.019	0.00000	16.189	0.288	0.54	35.52	2.65	42.773	1.098
800	4.689	0.012	0.00000	5.377	0.362	0.97	65.69	3.08	49.678	0.673
833	3.337	0.014	0.01746	3.060	0.727	1.83	72.33	2.41	39.049	0.377
866	3.145	0.013	0.00657	1.770	0.884	2.88	82.75	2.60	42.072	0.281
900	2.301	0.012	0.00049	0.886	1.637	4.83	87.75	2.02	32.719	0.210
933	2.078	0.013	0.00264	0.807	2.450	7.74	87.56	1.82	29.509	0.146
966	2.430	0.013	0.00157	0.830	3.616	12.03	89.09	2.17	35.065	0.087
1000	1.936	0.013	0.00146	0.560	6.417	19.66	90.43	1.75	28.408	0.063
1033	1.899	0.013	0.00084	0.470	9.644	31.11	91.63	1.74	28.233	0.074
1066	1.867	0.013	0.00049	0.325	14.149	47.92	93.79	1.75	28.411	0.064
1100	1.854	0.013	0.00083	0.265	20.374	72.12	94.70	1.76	28.481	0.051
1200	1.877	0.013	0.00709	0.218	20.805	96.84	95.53	1.79	29.081	0.048
1400	3.417	0.014	0.02543	5.051	2.660	100.00	55.78	1.91	30.902	0.134
TH258_Wm										
$J=0.009091$										
1	15.532	0.018	0.00362	6.039	0.215	10.47	88.41	13.73	212.225	0.872
2	15.523	0.012	0.00000	0.110	0.468	33.24	99.69	15.47	237.462	0.708
3	15.267	0.012	0.00139	0.214	0.528	58.89	99.48	15.19	233.331	0.343
4	14.982	0.013	0.00799	0.000	0.099	63.70	99.90	14.97	230.154	0.674
5	15.945	0.013	0.00892	0.550	0.242	75.47	98.89	15.77	241.663	0.588
6	15.775	0.014	0.00654	0.203	0.227	86.50	99.52	15.70	240.704	0.657
7	16.024	0.014	0.00798	0.139	0.101	91.43	99.65	15.97	244.539	1.197
8	15.653	0.009	0.02166	0.000	0.040	93.36	99.90	15.64	239.819	1.232
9	16.347	0.012	0.00823	0.000	0.059	96.21	99.90	16.33	249.744	1.288
10	16.401	0.012	0.01708	0.534	0.078	100.00	98.95	16.23	248.272	1.466
TH013_Kf										
$J=0.009065$										
400	6.963	0.018	0.00014	16.958	0.569	1.07	27.74	1.93	31.318	0.776
450	2.774	0.014	0.00169	3.761	1.536	2.15	59.22	1.64	26.670	0.232
450	2.308	0.013	0.00048	2.178	1.463	3.19	71.25	1.64	26.700	0.220
500	2.027	0.014	0.00150	1.123	2.856	5.20	82.65	1.68	27.194	0.127
500	1.932	0.013	0.00071	0.793	2.087	6.68	86.84	1.68	27.232	0.133
550	2.109	0.014	0.00095	0.676	3.069	8.84	89.58	1.89	30.635	0.128
550	2.014	0.013	0.00000	0.482	1.782	10.10	91.94	1.85	30.032	0.143
600	2.223	0.014	0.00066	0.733	2.373	11.78	89.36	1.99	32.201	0.093
600	2.071	0.014	0.00026	0.387	1.454	12.80	93.52	1.94	31.397	0.130
650	2.250	0.014	0.00132	0.497	1.991	14.21	92.59	2.08	33.748	0.134
650	2.140	0.013	0.00000	0.376	1.269	15.11	93.88	2.01	32.552	0.124
700	2.292	0.014	0.00209	0.865	1.829	16.40	87.98	2.02	32.681	0.129
700	2.861	0.016	0.00000	0.926	1.320	17.33	89.73	2.57	41.509	0.182
750	2.874	0.021	0.00205	1.066	2.546	19.13	88.35	2.54	41.048	0.133
750	2.876	0.023	0.00000	0.785	1.826	20.42	91.24	2.62	42.418	0.171
800	2.840	0.021	0.00058	0.754	2.386	22.10	91.45	2.60	41.979	0.110
800	3.068	0.024	0.00170	0.805	2.381	23.78	91.60	2.81	45.378	0.112
800	3.166	0.026	0.00099	1.057	2.399	25.48	89.51	2.83	45.754	0.098
850	2.857	0.022	0.00078	0.803	1.346	26.43	91.00	2.60	42.028	0.205
900	2.768	0.022	0.00371	0.829	3.081	28.60	90.44	2.50	40.477	0.144
950	2.708	0.022	0.00241	0.758	5.710	32.64	90.99	2.46	39.854	0.089
1000	2.708	0.022	0.00241	0.758	5.710	32.64	90.99	2.46	39.854	0.089
1000	2.667	0.022	0.00296	0.730	7.089	37.64	91.16	2.43	39.324	0.113
1050	2.624	0.024	0.00312	0.646	9.325	44.23	91.97	2.41	39.045	0.120
1100	2.834	0.026	0.00284	0.851	16.932	56.18	90.42	2.56	41.434	0.078
1200	3.258	0.025	0.00143	1.386	59.613	98.28	86.82	2.83	45.678	0.112
1400	3.582	0.021	0.00390	3.235	2.432	100.00	72.76	2.61	42.121	0.292
TH273_Kf										
$J=0.009065$										
400	30.557	0.082	0.02439	87.771	0.122	0.83	15.06	4.60	73.739	2.703
450	14.736	0.054	0.02859	36.912	0.350	1.68	25.86	3.81	61.259	1.086

(*continued on next page*)

Please cite this article as: Heymes, T., et al., Alpine tectonics in the Calabrian–Peloritan belt (southern Italy): New $^{40}Ar/^{39}Ar$ data in the Aspromonte Massif area, Lithos (2009), doi:10.1016/j.lithos.2009.10.011

Table 3 (*continued*)

Step	$^{40}Ar/^{39}Ar$	$^{38}Ar/^{39}Ar$	$^{37}Ar/^{39}Ar$	$^{36}Ar/^{39}Ar$ (E−3)	^{39}Ar (E−14)	$\%^{39}Ar$	$\%^{40}Ar^*$	$^{40}Ar^*/^{39}K$	Age (Ma)	Error
TH273_Kf										
$J = 0.009065$										
450	7.772	0.025	0.01867	15.759	0.313	2.43	39.84	3.10	49.943	1.197
500	7.462	0.032	0.02794	15.782	0.773	4.29	37.26	2.78	44.910	0.423
500	5.375	0.027	0.02404	8.237	0.588	5.71	54.38	2.92	47.181	0.562
550	6.092	0.028	0.03239	11.393	1.146	8.47	44.44	2.71	43.747	0.393
550	4.464	0.017	0.04167	5.818	0.767	10.32	61.10	2.73	44.061	0.448
600	6.032	0.026	0.04442	10.642	1.365	13.61	47.58	2.87	46.343	0.308
600	3.974	0.016	0.04204	3.774	0.841	15.64	71.50	2.84	45.879	0.327
650	4.718	0.021	0.04991	6.103	1.287	18.75	61.41	2.90	46.777	0.290
650	3.710	0.017	0.05241	2.673	0.783	20.63	78.25	2.90	46.864	0.296
700	4.362	0.022	0.06134	4.293	1.097	23.28	70.54	3.08	49.629	0.393
700	5.146	0.024	0.06874	3.369	0.744	25.07	80.35	4.14	66.388	0.519
750	5.753	0.051	0.09950	6.587	1.517	28.73	65.92	3.79	60.988	0.427
750	5.992	0.057	0.12813	6.653	0.911	30.93	66.98	4.01	64.473	0.392
800	6.168	0.047	0.11946	8.494	0.942	33.20	59.10	3.65	58.648	0.296
800	6.369	0.045	0.06898	8.789	0.846	35.24	58.98	3.76	60.410	0.356
800	7.153	0.049	0.05503	11.015	0.969	37.57	54.26	3.88	62.385	0.527
850	7.669	0.046	0.06501	12.997	0.904	39.75	49.71	3.81	61.300	0.467
900	6.701	0.045	0.06621	10.057	1.868	44.25	55.41	3.71	59.729	0.281
950	6.376	0.045	0.08390	9.145	2.904	51.26	57.38	3.66	58.868	0.316
1000	6.551	0.045	0.11015	9.438	3.502	59.70	57.22	3.75	60.284	0.261
1050	6.826	0.056	0.13207	9.046	4.567	70.71	60.66	4.14	66.487	0.233
1100	7.167	0.071	0.14769	8.956	6.147	85.53	62.92	4.51	72.287	0.166
1200	7.332	0.088	0.12785	6.432	5.392	98.53	73.91	5.42	86.518	0.322
1400	17.399	0.175	0.31400	19.299	0.610	100.00	67.22	11.70	181.818	1.141
TH276_Kfd										
$J = 0.008888$										
400	10.757	0.030	0.19418	29.938	0.505	11.09	17.68	1.90	30.250	0.817
400	4.386	0.015	0.18870	2.717	0.167	14.75	81.50	3.58	56.436	0.623
450	4.818	0.014	0.24044	5.444	0.153	18.11	66.50	3.20	50.661	1.100
450	4.677	0.014	0.26338	3.731	0.106	20.43	76.34	3.57	56.364	1.156
500	5.466	0.014	0.41667	5.649	0.123	23.12	69.56	3.80	59.972	1.090
500	5.128	0.016	0.46121	4.029	0.081	24.90	76.94	3.95	62.202	0.992
550	5.284	0.011	0.58328	5.420	0.094	26.97	69.98	3.70	58.363	1.081
550	5.093	0.014	0.70628	1.925	0.073	28.57	89.28	4.55	71.506	0.772
600	5.177	0.022	1.12067	6.334	0.106	30.89	64.77	3.36	53.027	1.101
600	6.181	0.031	1.40785	7.568	0.078	32.61	64.87	4.01	63.230	2.190
650	6.136	0.029	1.85787	8.931	0.088	34.53	58.50	3.59	56.725	2.015
650	6.080	0.024	1.60089	7.975	0.062	35.89	62.51	3.80	59.996	2.761
700	7.649	0.028	1.28194	13.059	0.094	37.94	50.30	3.85	60.715	1.178
700	6.714	0.014	0.77110	3.304	0.068	39.43	85.86	5.77	90.191	1.065
750	5.494	0.020	0.61174	5.615	0.110	41.85	70.11	3.85	60.753	0.854
750	5.805	0.016	0.50030	5.441	0.077	43.54	72.48	4.21	66.258	1.451
800	5.564	0.021	0.45471	6.188	0.113	46.03	67.27	3.74	59.050	0.930
800	5.674	0.014	0.42843	7.137	0.082	47.84	62.94	3.57	56.384	1.152
800	5.813	0.011	0.36347	6.134	0.079	49.58	68.85	4.00	63.070	1.324
800	6.924	0.005	0.42212	4.256	0.039	50.43	81.91	5.67	88.746	1.066
850	5.912	0.020	0.41843	8.522	0.092	52.44	57.49	3.40	53.706	1.120
900	4.966	0.019	0.40314	6.699	0.240	57.70	60.23	2.99	47.348	0.598
950	4.588	0.023	0.42939	6.596	0.459	67.77	57.65	2.65	41.936	0.372
1000	6.253	0.035	0.79693	12.842	0.609	81.12	39.76	2.49	39.453	0.435
1050	10.790	0.068	1.86055	27.601	0.528	92.68	25.27	2.73	43.254	0.458
1100	17.852	0.129	4.57206	45.819	0.194	96.92	25.60	4.58	72.033	1.326
1200	33.964	0.315	12.38719	78.784	0.090	98.87	33.60	11.51	175.662	3.015
1400	50.416	0.442	7.08022	121.213	0.052	100.00	29.77	15.08	226.860	5.418

Absolute errors are given at the 1σ confidence level.

of a real plateau is probably due to the effects of late recrystallization and coeval chemical heterogeneity of the dated white mica bulk separate, as illustrated by variations in celadonite content and the probable presence of paragonite interlayers (Table 2 and Fig. 5a). The intercept age (33.7 ± 0.6 Ma) in the $^{36}Ar/^{40}Ar$ versus $^{39}Ar/^{40}Ar$ diagram is close to the pseudo-plateau age confirming its probable reliability despite a high MSWD (7.70) and an $^{40}Ar/^{36}Ar$ initial ratio of 263 ± 5, somewhat different from the present-day atmospheric ratio of 295.5 (e.g., McDougall and Harrison, 1999).

For sample TH157, the age spectrum displays a saddle-shaped pattern. The main portion of this spectrum yields a pseudo-plateau age of 32.7 ± 0.3 Ma calculated on three successive steps corresponding to 76% of the total gas released (Fig. 6e). The pseudo-plateau age is very close to the total fusion age of 33.7 ± 0.1 Ma. Chemical heterogeneities in the bulk separate are suggested by K/Ca variations during step heating, even though microprobe analyses indicate the absence of such Ca/K variations (Table 2). A minor contamination by plagioclase or epidote is probably responsible for this variable Ca content. The inverse isochron age (33.1 ± 0.6 Ma; MSWD = 4.47) is very close to the pseudo-plateau and total fusion ages and confirms their reliability. The high value (325 ± 10) of the $^{40}Ar/^{36}Ar$ intercept probably results of excess argon contamination producing the saddle-shape of the age spectrum.

Sample TH164 provided a saddle-shaped spectrum with a pseudo-plateau age of 32.8 ± 0.3 Ma, defined by six successive steps

Please cite this article as: Heymes, T., et al., Alpine tectonics in the Calabrian–Peloritan belt (southern Italy): New $^{40}Ar/^{39}Ar$ data in the Aspromonte Massif area, Lithos (2009), doi:10.1016/j.lithos.2009.10.011

Table 4
$^{40}Ar/^{39}Ar$ results.

Sample	Unit	Analysis	Total fusion age	Pseudo-plateau age	%^{39}Ar	Intercept age	MSWD	$^{40}Ar/^{36}Ar$	Method
Ca02-113	APU	Ca02-113-Wm	37.7 ± 0.1	36.3 ± 0.6	(84)	**36.3 ± 0.4**	2.86	319 ± 1	Laser
TH013	AU	TH013-Kf	41.4 ± 0.4	–	–	**27.0 ± 0.4**	1.92	309 ± 4	Furnace
TH109	AU	TH109-Wm	138 ± 1.3	–	–	–	–	–	Furnace
TH111	APU	TH111-Wm	255 ± 2.4	–	–	–	–	–	Furnace
TH140	APU	TH140-Wm	32.3 ± 0.1	**33.0 ± 0.3**	(77)	33.7 ± 0.6	7.70	263 ± 5	Furnace
TH157	APU	TH157-Amp	147 ± 1.0	–	–	–	–	–	Furnace
		TH157-Wm	33.7 ± 0.1	**32.7 ± 0.3**	(76)	33.1 ± 0.6	4.47	325 ± 10	Furnace
TH164	APU	TH164-Amp	145 ± 1.6	–	–	–	–	–	Furnace
		TH164-Wm1	33.8 ± 0.3	32.8 ± 0.3	(81)	**33.6 ± 0.5**	2.83	290 ± 10	Furnace
		TH164-Wm2	70.3 ± 0.5	33.7 ± 1.3	(44)	**33.2 ± 0.8**	0.59	334 ± 21	Laser
TH258	SU	TH258-Wm	235 ± 0.2	–	–	–	–	–	Laser
TH269	AU	TH269-Wm1	26.3 ± 0.2	28.5 ± 0.3	(53)	**29.2 ± 0.5**	4.15	276 ± 5	Furnace
		TH269-Wm2	29.4 ± 0.2	**28.7 ± 0.3**	(85)	28.6 ± 0.4	2.57	345 ± 8	Furnace
TH273	AU	TH273-Kf	66.2 ± 0.6	–	–	**45.0 ± 1.0**	7.99	314 ± 5	Furnace
TH276	AU	TH276-Kf	54.6 ± 0.2	–	–	44.6 ± 4.0	22.9	289 ± 23	Furnace

APU: Africo-Polsi Unit; AU: Aspromonte Unit; SU: Stilo Unit; ages are given in Ma; preferred ages are highlighted by bold print.

corresponding to 81% of the total gas released (Fig. 6f) and in agreement with the total fusion age (33.8 ± 0.3 Ma). During the last heating steps, apparent ages reached a maximum value of 180 ± 17 Ma. The saddle-shaped spectrum indicates that argon was released from different reservoirs, as suggested by the K/Ca plot, the presence of paragonite interlayers (Table 2) and the significant scattering of data in the $^{36}Ar/^{40}Ar$ versus $^{39}Ar/^{40}Ar$ isotope diagram. However, the concordance of the inverse isochron age of 33.6 ± 0.5 Ma (MSWD = 2.83; $^{40}Ar/^{36}Ar = 290 \pm 10$) with the pseudo-plateau and total fusion ages allows us to consider it as a reliable age estimate for the isotopic closure of white mica.

In addition, a laser-probe analysis was carried out on a single grain from the same sample (Fig. 6g). Ages range from 24.9 ± 4.8 Ma at low temperature to 119 ± 0.9 Ma at high temperature for a total fusion age of 70.3 ± 0.5 Ma, significantly older than the total fusion age of the bulk separate. A pseudo-plateau of 33.7 ± 1.3 Ma has been calculated for an intermediate portion of this spectrum (steps 2 to 6; 44% of total gas released), in agreement with an inverse isochron age of 33.2 ± 0.8 Ma (MSWD = 0.59; $^{40}Ar/^{36}Ar = 334 \pm 21$). According to the age, K/Ca and Cl/K variations, it is likely that this larger grain is composed of several overgrowths (or intergrowths) of white mica with a significant inheritance of an older radiogenic component. This component is less obvious in the bulk separate analysis, probably because this separate consists of a mixture of mainly fine-grained, newly formed white mica plus some broken grains similar to that dated with the laser probe.

The last sample (Ca02-113) is from the western part of the Africo-Polsi Unit, in the Cardeto area. Its analysis yielded a saddle-shaped age spectrum (Fig. 6h) with ages ranging from 35.7 ± 0.1 Ma to 71.2 ± 5.5 Ma and a total fusion age of 37.7 ± 0.1 Ma. For the three main heating steps, corresponding to 84% of the total gas released, we calculated a pseudo-plateau age of 36.3 ± 0.6 Ma which is equivalent to the inverse isochron age (MSWD = 2.86; $^{40}Ar/^{36}Ar = 319 \pm 1$). Again, the discordant K/Ca diagram and the paragonite content (Table 2) of this sample suggest that several argon reservoirs participated to the argon release, resulting in the saddle-shape age pattern.

4.2.2. Aspromonte Unit

4.2.2.1. White micas. Sample TH109 yielded a staircase-shaped age spectrum with ages progressively increasing from 42.8 ± 3.7 Ma to 155 ± 1.1 Ma (Fig. 6i) and a total fusion age of 138 ± 0.1 Ma. Significant chemical heterogeneity within the dated white mica bulk separate is evidenced by the K/Ca ratio variations. Due the large scattering of the data, no significant intercept age was obtained in the $^{36}Ar/^{40}Ar$ versus $^{39}Ar/^{40}Ar$ diagram.

In contrast, a duplicate analysis of sample TH269, from the same shear zone, but in a lower level of the tectonic pile, yielded more significant results. The age spectrum derived from a first bulk separate of white mica (Fig. 6j) shows a relatively discordant pattern with ages ranging from 8.7 ± 0.6 Ma to 793 ± 240 Ma and a total fusion age of 26.3 ± 0.2 Ma. The latter is similar to a pseudo-plateau age of 28.5 ± 0.3 Ma, calculated on two successive steps representing 53% of the total gas released and to the inverse isochron age of 29.2 ± 0.5 Ma (MSWD of 4.15; $^{40}Ar/^{36}Ar = 276 \pm 5$).

The second bulk separate yielded a less discordant age spectrum with ages ranging from 28.2 ± 0.1 Ma to 49.6 ± 0.7 Ma (Fig. 6k), for a total fusion age of 29.4 ± 0.3 Ma. A plateau age of 28.7 ± 0.3 Ma was calculated on five steps corresponding to 85% of the total argon released, in agreement with an intercept age of 28.6 ± 0.4 Ma (MSWD of 2.57; $^{40}Ar/^{36}Ar = 345 \pm 8$). Significant variations of the K/Ca ratio suggest that several reservoirs contributed to the gas released during step heating, with some of the steps being contaminated by excess argon as indicated by the high initial argon ratio in the isotope correlation plot.

4.2.2.2. K-feldspars. For K-feldspars, we duplicated isothermal step heating at low temperatures in order to identify excess argon from possible fluid inclusions and to evaluate the contribution of the different argon reservoirs. As shown on Fig. 6, the three studied samples (TH013, TH273 and TH276) yielded very discordant age spectra and K/Ca and Cl/K patterns that probably result from the simultaneous degassing of several textural and chemical microdomains, as well as fluid or solid inclusions within the K-feldspar population (see e.g. Burgess et al., 1992; Harrison et al., 1994; McLaren and Reddy, 2008).

The age spectrum of sample TH013 (Fig. 6l) shows a progressive increase of apparent ages from a minimum age of 26.6 ± 0.2 Ma to a maximum age of 45.7 ± 0.1 Ma, for a total fusion age of 41.4 ± 0.4 Ma. For this sample, the age variations are broadly mirrored by the K/Ca and Cl/K spectra and no plateau segment can be identified. These different isotopic patterns suggest that inclusions responsible for excess argon were mainly decrepitated during the first heating steps below ~35% of the gas released. For the very first steps, an intercept age of 27.0 ± 0.4 Ma has been obtained in the $^{36}Ar/^{40}Ar$ versus $^{39}Ar/^{40}Ar$ diagram using 6 heating steps (MSWD of 1.92; $^{40}Ar/^{36}Ar = 309 \pm 4$). By comparison, the age spectrum of sample TH273 is relatively less discordant (Fig. 6m), with a weaker contribution of excess argon at low temperature. Discarding the excess argon effects, ages increase from 44.9 ± 0.4 to 86.5 ± 0.3 Ma, for a total fusion age of 66.2 ± 0.6 Ma. The low-temperature portion of this spectrum corresponds to an inverse isochron age of 45.0 ± 1.0 Ma calculated on 13 heating steps (MSWD of 7.99; $^{40}Ar/^{36}Ar = 314 \pm 5$).

Please cite this article as: Heymes, T., et al., Alpine tectonics in the Calabrian–Peloritan belt (southern Italy): New $^{40}Ar/^{39}Ar$ data in the Aspromonte Massif area, Lithos (2009), doi:10.1016/j.lithos.2009.10.011

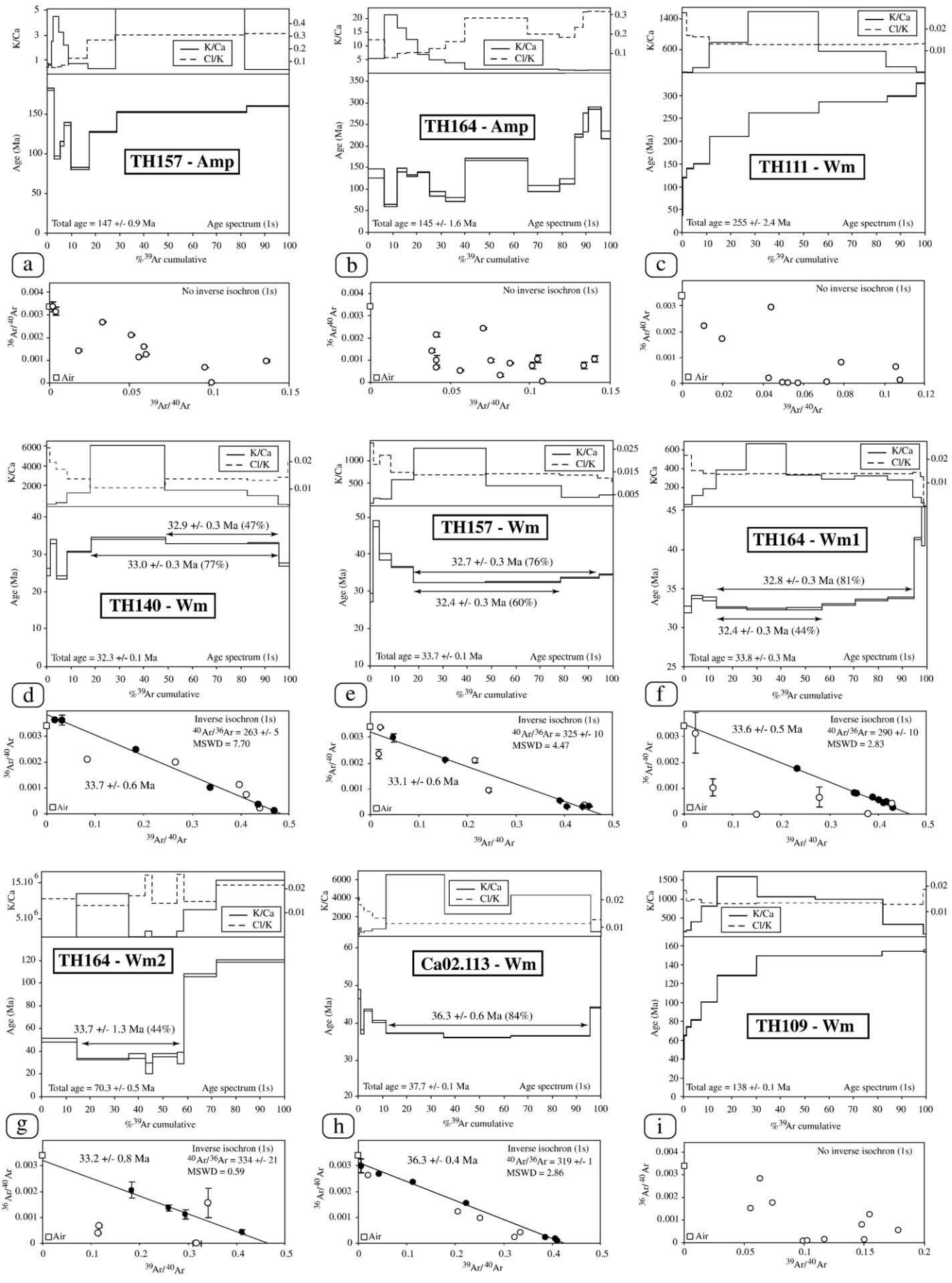

Please cite this article as: Heymes, T., et al., Alpine tectonics in the Calabrian–Peloritan belt (southern Italy): New $^{40}Ar/^{39}Ar$ data in the Aspromonte Massif area, Lithos (2009), doi:10.1016/j.lithos.2009.10.011

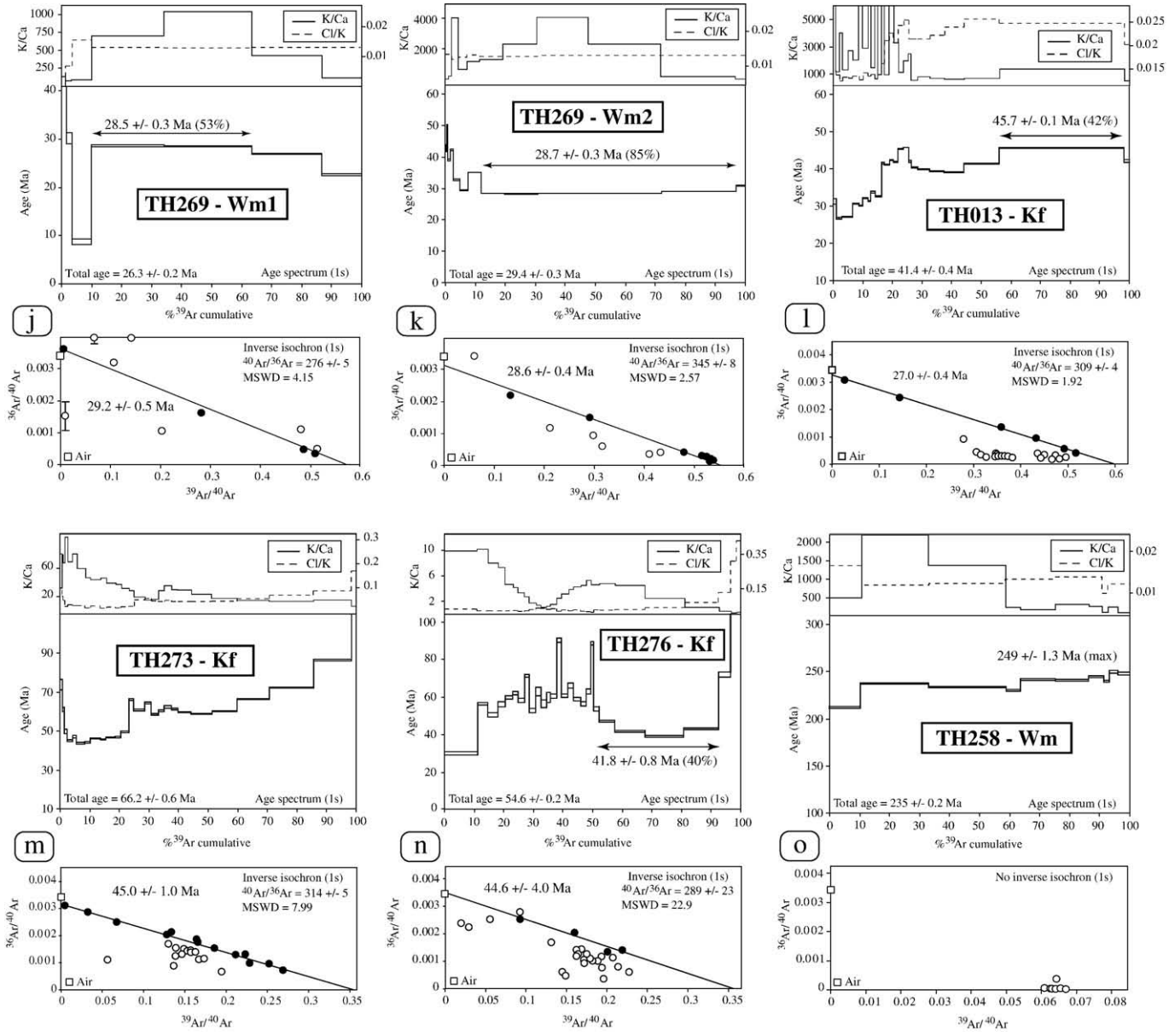

Fig. 6. K/Ca and Cl/K diagrams, age spectrum and $^{36}Ar/^{40}Ar$ versus $^{39}Ar/^{40}Ar$ diagram obtained for each sample. See Table 3 for details.

The last K-feldspar (sample TH276) provided a very scattered age spectrum (Fig. 6n) with ages ranging from 30.2 ± 0.8 Ma to 226 ± 5.4 Ma for the last step, and a total fusion age of 54.6 ± 0.2 Ma. The majority of individual ages are in the range of 30–60 Ma, with a clear contribution of excess argon from inclusions, released at low and intermediate experimental temperatures. At high temperatures, the age spectrum displays a saddle-shaped pattern with a minimum integrated age on three steps of 41.8 ± 0.8 Ma, corresponding to 40% of the total gas released. A similar intercept age of 44.6 ± 4.0 Ma is provided by the $^{36}Ar/^{40}Ar$ versus $^{39}Ar/^{40}Ar$ diagram, but the large MSWD value (23) makes the meaning of this age very questionable, even if its consistency with the isochron age of sample TH273 is noticeable. The variations of the K/Ca ratio suggest that the dated bulk separate consists of a mixture of chemically different subgrains with excess argon mainly related to the low K/Ca domains.

These results reveal strong heterogeneity within the K-feldspars analyzed, with the presence of complex inherited and excess argon reservoirs. These disturbances probably result from the complex geological history marked by a succession of several thermal (Hercynian and Alpine) events, (re)crystallization and fluid impregnation phases. For these reasons, we refrained from employing multi-domain thermal modelling of K-feldspars following the method of Lovera (1992). In the following, we consider the low-temperature portion of an age spectrum unaffected by excess argon as recording cooling at about 150 °C while the high temperature portion provided mixed ages that cannot be correlated with a precise cooling step.

4.2.3. Stilo Unit

The age spectrum derived from a single muscovite grain of sample TH258 does not show a significant plateau segment (Fig. 6o) but a series of ages increasing from 212 ± 0.8 Ma to 249 ± 1.3 Ma for a total fusion age of 235 ± 0.2 Ma. Due to a very high radiogenic yield, the data points cluster near the abscissa in the $^{36}Ar/^{40}Ar$ versus $^{39}Ar/^{40}Ar$ diagram, precluding calculation of a meaningful inverse isochron age.

Please cite this article as: Heymes, T., et al., Alpine tectonics in the Calabrian–Peloritan belt (southern Italy): New $^{40}Ar/^{39}Ar$ data in the Aspromonte Massif area, Lithos (2009), doi:10.1016/j.lithos.2009.10.011

5. Discussion

5.1. Geological interpretation of the $^{40}Ar/^{39}Ar$ data

Interpreting $^{40}Ar/^{39}Ar$ data in relatively low-temperature metamorphic rocks generally poses the question of whether these data record cooling or crystallization ages (e.g. Dunlap, 1997; Mulch and Cosca, 2004). The answer depends on the *PT* path recorded by these rocks and the closure temperature adopted for the K–Ar system in the considered minerals. In addition, several effects due to the polyphase evolution of the rocks, the presence of excess argon or the preservation of inherited argon in relict minerals (even for temperatures above the closure temperature of these minerals; e.g., Maurel et al., 2003) can drastically alter this simple way of interpreting argon results as recording crystallization and cooling processes only. Therefore, keeping in mind that the interpretation of geochronological data is not straightforward, the following closure temperatures for argon have been adopted: 450–400 °C for the muscovite–phengite mica group (e.g. Hames and Bowring, 1994; Agard et al., 2002), 550–500 °C for amphibole (e.g. Dahl, 1996), and 350–150 °C for K-feldspar multi-domain systems (e.g. Lovera et al., 1989; Arnaud et al., 1993).

5.1.1. Evidence for pre-Alpine metamorphism in the Africo-Polsi Unit

The new geochronological results reported here are the first $^{40}Ar/^{39}Ar$ data published for the Aspromonte Massif. Previous geochronological studies in the southern Calabrian–Peloritan belt have shown that the tectonometamorphic evolution is polyphase, with clear evidence for superposition of Hercynian and Alpine events (Bonardi et al., 1987; Graessner et al., 2000; De Gregorio et al., 2003). In the Aspromonte and Stilo units, the Hercynian tectonometamorphic evolution is well documented (see Section 2.2). In the Africo-Polsi Unit, our data suggest a pre-Alpine metamorphic imprint that is best preserved away from the main Alpine tectonic contacts. Geochronological data of blue–green amphiboles from samples TH157 and TH164 cannot be interpreted in terms of cooling ages but only as mixed ages since these amphiboles are pre-Alpine relicts partially recrystallized during Alpine metamorphism. A similar interpretation can be proposed for white micas from TH111 from the uppermost (southern) part of the Africo-Polsi Unit. The staircase-shaped age spectrum obtained for this sample likely reflects the mixture of pre-Alpine and Alpine micas as has been described elsewhere in the Alpine belt (e.g. Wijbrans and McDougall, 1986; Monié, 1990). Pre-Alpine minerals suffered only partial resetting during very low-grade Alpine metamorphism in this area of the Africo-Polsi Unit. The Alpine foliation in this sample probably transposed an older low-temperature Hercynian foliation, resulting in re-orientation and partial recrystallization of older Hercynian muscovite and syn-kinematic growth of a tiny Alpine mica generation, with both generations of minerals having nearly the same composition close to that of muscovite.

5.1.2. Age of Alpine metamorphism

In contrast, white micas (samples TH140, TH157 and TH164) from the lowermost (northern) part of Africo-Polsi Unit experienced higher Alpine metamorphic conditions than in those from the southern part, and yielded less disturbed age spectra with little or no evidence of inherited argon. The three samples yielded very similar intercept ages of 33–34 Ma in the reverse correlation diagram, interpreted to date cooling below temperatures in the range of 400–450 °C. In the western part of the Aspromonte Massif, micas from sample Ca02-113 yielded an intercept age of about 36 Ma that suggests cooling occurred somewhat earlier there than in the northern part of the Africo-Polsi Unit.

Given the *PT* path suggested for this unit (Fig. 7), it is very likely that cooling occurred shortly after the isothermal decompression that accompanied exhumation of the Africo-Polsi Unit from a depth of about 30 km to about 10 km (Cirrincione et al., 2008). However, this *PT* reconstruction must be considered with some caution because it was obtained under the assumption that all mineralogical assemblages in the Africo-Polsi Unit are Alpine, which is partly contradicted by our geochronological data. Both *P* and *T* conditions may have been overestimated by Cirrincione et al. (2008) due to the fact that the minerals used for these estimates do not exhibit mutual compositional equilibrium. Our as yet unpublished preliminary estimates using chlorite–phengite multiequilibrium calculations (Vidal and Parra, 2000) suggest lower *P* and *T* conditions than those proposed by Cirrincione et al. (2008), most probably in the range of 450–550 °C and 6–9 kbar for the deepest part of the Africo-Polsi Unit. Therefore, the 33–34 Ma ages reported in this unit could be much closer to the metamorphic peak than assumed using the estimates of Cirrincione et al. (2008). Additional petrological investigations are needed to get a better picture of the *PT*-t path in this unit.

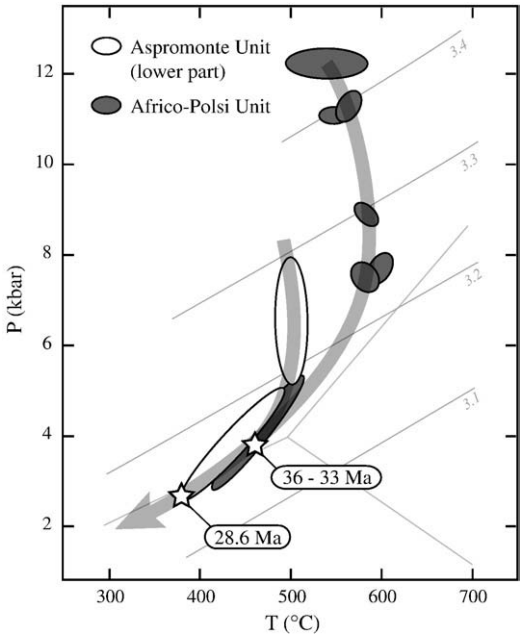

Fig. 7. *PT* estimates for the Aspromonte (lower part) and Africo-Polsi units during Alpine metamorphic overprint (after Messina et al., 1992 and Cirrincione et al., 2008). Si content isopleths from white micas are reported as indicative after Massonne and Schreyer (1987). The ages obtained during this study are reported at corresponding inferred positions on the exhumation path, figured by the large grey arrow.

Nonetheless, these Lower Oligocene ages are similar to those reported in the ophiolitic units of northern Calabria (Rossetti et al., 2004) and are likely related to a major step in the Alpine metamorphic evolution of the Africo-Polsi Unit. As most of the dated white micas belong to a single Alpine foliation, which is associated with the initial stage of stacking and which remained mostly unaffected by the less penetrative late extensional shear zones, the ages of 33–36 Ma most probably correspond to the time the rocks were brought to upper crustal levels after the main stacking episode.

5.1.3. Age of the late extensional shear zones

The fabric of the two main regional contacts identified in the Aspromonte Massif was acquired during the extensional reactivation of the tectonic pile (Heymes et al., 2008). White micas separated from mylonitic gneisses at the base of the Aspromonte Unit yielded contrasting results.

Sample TH109 was collected in the uppermost part of the pile. Both the mylonitic microfabric and the low-grade greenschist-facies metamorphism of the nearby underlying Africo-Polsi Unit suggest that Alpine temperatures were too low to allow complete recrystallization and resetting of older minerals. The staircase-shaped age spectrum (40–155 Ma) we obtained is probably due to mixing of two generations of white mica, the older one suffering only partial isotopical resetting during Alpine deformation.

Please cite this article as: Heymes, T., et al., Alpine tectonics in the Calabrian–Peloritan belt (southern Italy): New $^{40}Ar/^{39}Ar$ data in the Aspromonte Massif area, Lithos (2009), doi:10.1016/j.lithos.2009.10.011

On the other hand, the duplicate analysis of white micas from a highly recrystallized mylonite (sample TH269) yielded two very consistent ages around 28.6 Ma that, given to the low-temperature conditions prevailing during shearing, are interpreted to date the main fabric of this rock. This age is 4–7 Ma younger than the age of the main post-stacking exhumation in the underlying Africo-Polsi Unit, in contrast to the age pattern observed in most metamorphic complexes. The age pattern indicates that rocks of the Africo-Polsi Unit had already cooled through the closure temperature for argon in white mica (400–450 °C) when shearing was active in the overlying Aspromonte Unit. Our results demonstrate that white micas in the deepest mylonites of this unit have been completely recrystallized during extensional tectonics, as already suggested by petrographic observations and chemical analyses (see Section 3.2). At higher structural levels in the pile, however, the same deformation led to only partial resetting of white micas (sample TH258).

5.1.4. Age of exhumation of the Aspromonte Unit

According to Thomson (1994), the top of the Aspromonte Unit in the southern part of the massif was exhumed at 33 Ma (apatite fission-track ages). Our analyses on K-feldspar yield some additional constraints.

The two southernmost samples TH273 and TH276 display complex isotopic age patterns. No meaningful plateau segments have been identified but, for both samples, an intercept age of about 45 Ma has been obtained in the reverse isotope correlation plot. However, for sample TH273, this age is derived from the low-temperature portion of the age spectrum while for sample TH276, this age comes from the high-temperature part. For this second sample, the presence of significant excess argon, released at low to intermediate temperatures renders the 45 Ma age somewhat suspect. Considering only sample TH273, its age of 45 ± 1 Ma can be interpreted to reflect isotopic closure of K-feldspar at a temperature most probably in the range of 150–200 °C (Lovera et al., 1989; Arnaud et al., 1993). This age is consistent with the 33 Ma apatite fission-track ages (Thomson, 1994), which record cooling through a temperature of ~110 °C. Older ages provided by K-feldspars are related to the degassing of different reservoirs containing both excess and inherited argon, given the Hercynian age of the protolith.

The third sample (TH013) yielded a low-temperature intercept age of 27 Ma, showing that the time of its cooling through 150–200 °C is significantly younger than that of sample TH273. This younger age can be due to its deeper position in the central part of the massif, where the covering Stilo Unit was thicker. In addition, the total gas and maximum ages of sample TH013 are younger than those of sample TH273, which is also interpreted to reflect a deeper structural origin of sample TH013 compared to that of sample TH273, and more significant resetting of the argon chronometer in Alpine times for this sample. The low-temperature age of TH013 is consistent with the 28.6 Ma age of white mica from extensional shear zones in the deepest part of the Aspromonte Unit (sample TH269), implying tectonic separation of the Stilo and Aspromonte units during Late Oligocene times.

These new geochronological data are in agreement with the age of the oldest post-orogenic sediments: on the basis of biostratigraphic studies, the lowermost levels of the Stilo Capo d'Orlando formation (Bonardi et al., 1980), which seal the extensional tectonic contacts, were deposited during the Late Oligocene (Weltje, 1992) or Early Miocene according to more recent estimations (Bonardi et al., 2003) (Fig. 8).

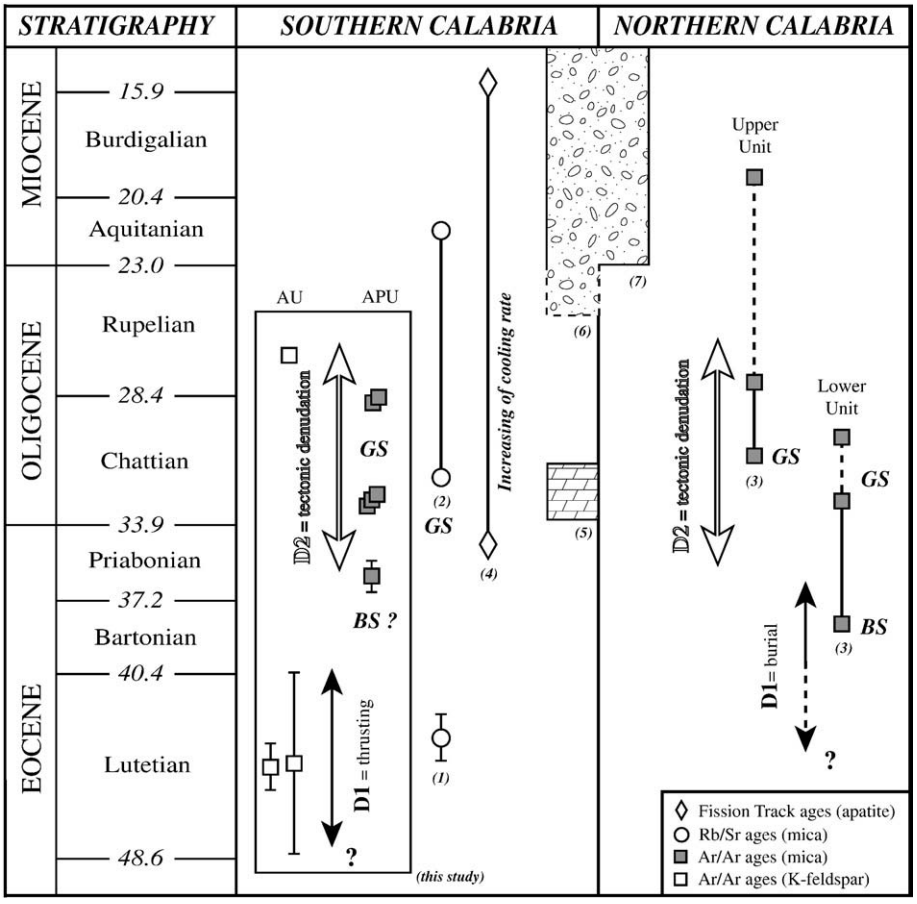

Fig. 8. Compilation of available chronological constraints for the Alpine tectonometamorphic evolution in the two main domains of the Calabrian–Peloritan belt. For each geochronological study, the method and mineral used (see legend box in the lower-right corner) and approximate metamorphic climax (BS: blueschist-facies conditions, GS: greenschist-facies conditions) are given. Studies are listed as follows: (1) Schenk (1980); (2) Bonardi et al. (1987); (3) Rossetti et al. (2004); (4) Thomson (1994). Syn- and post-orogenic sediments are reported at corresponding age positions according to (5) Bouillin (1985); (6) Weltje (1992) and (7) Bonardi et al. (2003). AU: ages from the Aspromonte Unit; APU: ages from the Africo-Polsi Unit and from the shear zone at the base of the Aspromonte Unit.

Please cite this article as: Heymes, T., et al., Alpine tectonics in the Calabrian–Peloritan belt (southern Italy): New $^{40}Ar/^{39}Ar$ data in the Aspromonte Massif area, Lithos (2009), doi:10.1016/j.lithos.2009.10.011

5.2. Timing of deformation stages and Alpine kinematics in the Calabrian–Peloritan belt

In southern Calabria, structural data (see Heymes et al., 2008) suggest that the Alpine tectonic evolution from shortening to extension shows many similarities with that recorded in northern Calabria (Fig. 8). Within the ophiolitic Liguride Complex of northern Calabria, the top-to-ENE stacking phase is dated between 38 and 33 Ma, while top-to-NW extensional reworking is more precisely dated around 30 Ma ($^{40}Ar/^{39}Ar$ dating on white micas; Rossetti et al., 2001; Rossetti et al., 2004) (Fig. 9). In southern Calabria, our geochronological study in the Aspromonte Massif provides new age constraints on the Alpine evolution of the Calabride Complex. The top-to-SE stacking phase was probably initiated before 45 Ma (Late Eocene), as suggested by the K-feldspar ages from different structural levels in the Aspromonte Unit. The top-to-NE extensional reworking of the pile is dated at 28.6 Ma (middle Oligocene), but our data indicate that the deepest units were partly exhumed since the Early Oligocene (36–33 Ma). This could suggest that the exhumation of southern Calabria was accommodated by several tectonic pulses from 45 to 28.6 Ma, with significant kinematic changes in this interval. West of the Aspromonte Massif, in the Peloritan Mountains of Sicily, the tectonic evolution of the Calabride Complex is similar but both kinematic directions and ages for successive steps are poorly constrained (Somma et al., 2005). To the north-east of the Aspromonte Massif, Langone et al. (2006) describe a major shear zone corresponding to a top-to-SE Alpine thrust surface, dated around 43 ± 1 Ma (Rb/Sr dating on micas; Schenk, 1980), which reinforces our interpretation of the 45 Ma ages in the Aspromonte Unit as representing the stacking phase (Fig. 9).

According to our recent paleotectonic reconstruction of the Western Mediterranean in the Lower Oligocene (Heymes et al., 2008), the Eocene–Oligocene top-to-SE direction of shortening is constant along the belt (Fig. 10). This direction is consistent with the local convergence direction proposed by geodynamic models for Eocene times (e.g. Jolivet and Faccenna, 2000; Faccenna et al., 2001), in which convergence is related to the closure of the Tethyan Ligurian–Piemontais oceanic domain. This early Alpine shortening is probably associated with the formation of an accretionary complex involving both oceanic and southern-European continental units. The age of ~45 Ma proposed in this study is close to the oldest ages obtained for the HP metamorphic climax of units from the conjugate extensional margin of Corsica–Sardinia block (45 to 35 Ma; Brunet et al., 2000).

Geodynamic models for the evolution of the Western Mediterranean suggest that the progressive eastward or southeastward retreat of the Ionian oceanic slab since ~30 Ma is the driving mechanism of extension (e.g. Jolivet and Faccenna, 2000; Faccenna et al., 2001). This extension begins with the NW–SE opening of the Ligurian–Provencal Basin, accommodated by counterclockwise rotation of the Corsica–Sardinia block. Crustal thinning at this time is also recorded by calcalkaline volcanism along the Sardinian and Provencal margins (Seranne, 1999; Faccenna et al., 2002; Lustrino et al., 2007). However, in the Calabrian–Peloritan belt, which is part of the Corsica–Sardinia block, our new ages combined with the paleotectonic reconstruction of Heymes et al. (2008) show an active extensional phase around 28.6 Ma

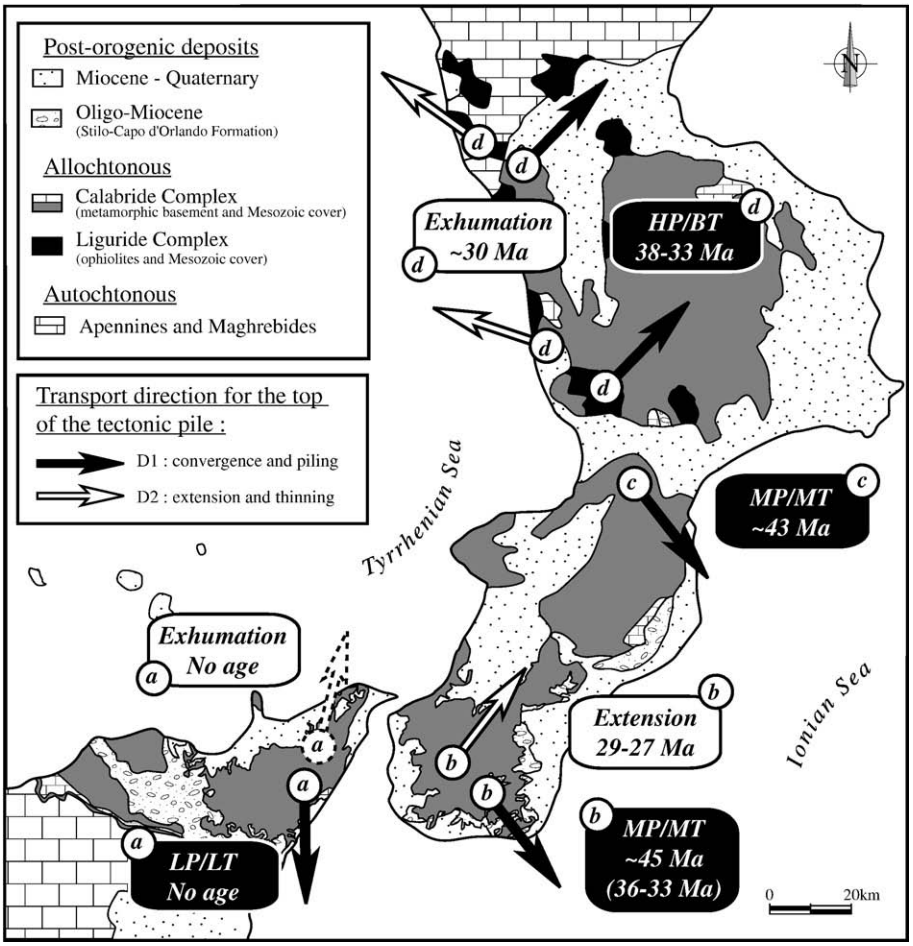

Fig. 9. Displacement directions, ages and approximate metamorphic conditions of the two successive phases of Alpine tectonics in the Calabrian–Peloritan belt. Stacking phase: black arrows; extensional phase: white arrows. (a) After Somma et al. (2005); (b) Heymes et al. (2008) and this study; (c) after Schenk (1980) and Langone et al. (2006); (d) after Rossetti et al. (2001) and Rossetti et al. (2004).

Please cite this article as: Heymes, T., et al., Alpine tectonics in the Calabrian–Peloritan belt (southern Italy): New $^{40}Ar/^{39}Ar$ data in the Aspromonte Massif area, Lithos (2009), doi:10.1016/j.lithos.2009.10.011

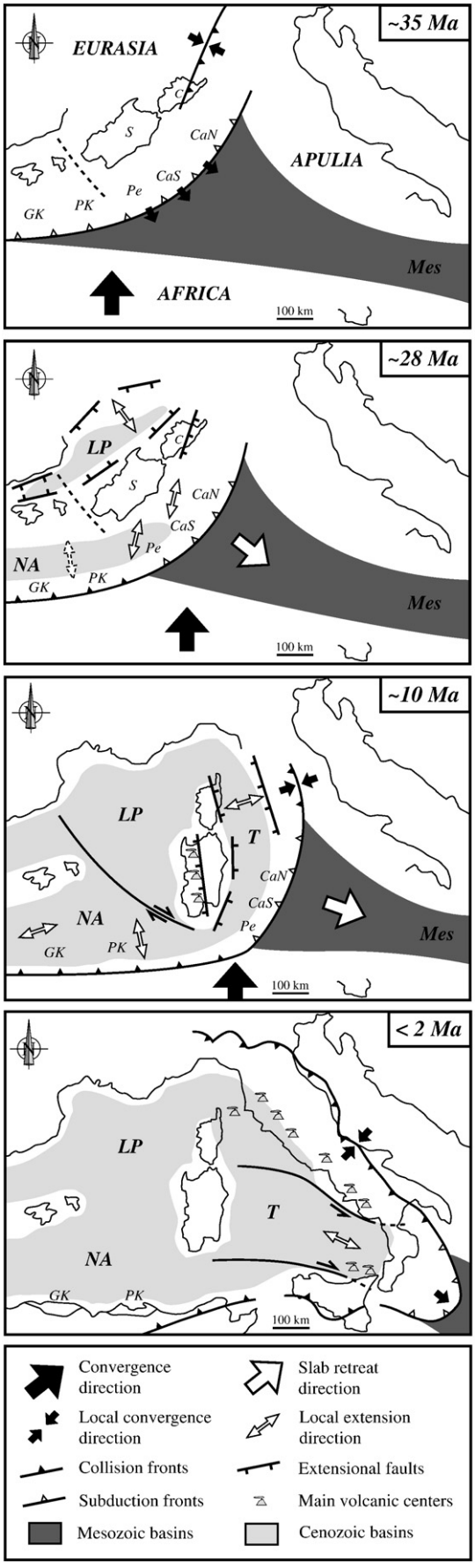

(middle Oligocene) oriented NNE–SSW rather than NW–SE (Fig. 10). Such kinematics fits better with N–S stretching of the southern-European margin, which probably resulted in the progressive opening of the North-Algerian Basin. In fact, to the west, a structural evolution similar to that of the Calabrian–Peloritan belt has been documented in the Sardinia channel (Bouillin et al., 1998; Mascle et al., 2004) and in the Kabylian massifs of Algeria, where (1) extensional reworking of the nappe pile from 24 Ma onward was partly controlled by a large detachment fault (Monié et al., 1988; Saadallah and Caby, 1996; Caby et al., 2001) and (2) the incorporation of peridotites into the Hercynian crust, dated at around 18 Ma, is supposed to be associated with the incipient rifting phase that accompanied opening of the North-Algerian Basin (Bruguier et al., 2009).

6. Conclusions

Our geochronological study reports the first $^{40}Ar/^{39}Ar$ data of the Aspromonte Massif of southern Calabria. These new data constrain the age of the transition between convergence and extension in a key area of the Western Mediterranean. The exhumation of units forming the upper part of the Calabride Complex probably initiated at ~45 Ma. Their structural position at the top of the nappe pile suggests that this cooling probably results from stacking stages within the orogenic wedge, built up along the NW-directed subduction zone of the Tethyan oceanic domain below the southern-European margin. Kinematic criteria indicate that this stacking was probably coeval with a top-to-SE displacement of the units. Their subsequent exhumation was dated at 36–33 Ma in the deepest unit of the Aspromonte Massif, while the final extensional stage affecting the entire tectonic pile has been more precisely dated around 28.6 Ma in deeper levels and around 27 Ma in shallower levels.

Eastward slab retreat is generally considered as the driving mechanism for the roughly E–W opening of the Ligurian–Provencal and Tyrrhenian Sea basins. Our combined structural and geochronological data show that the tectonic denudation observed in the Calabrian–Peloritan belt at middle Oligocene was directed NNE–SSW rather than NW–SE. We propose that this extension could be an eastward expression of N–S opening of the North-Algerian Basin during Oligocene times.

Acknowledgements

The French–Italian program “Vinci” is thanked for the financial support granted for the PhD thesis of the first author. We are grateful to F. Senebier for mineral separation, O. Romeyer and C. Groppo for SEM imagery and P. van der Beek for suggestions and considerable improvement of English expression. We thank the Associate Editor I.S. Buick, S. McLaren and an anonymous reviewer for their constructive comments on the manuscript.

References

Agard, P., Monié, P., Jolivet, L., Goffé, B., 2002. Exhumation of the Schistes Lustrés complex: in situ laser probe Ar-40/Ar-39 constraints and implications for the Western Alps. Journal of Metamorphic Geology 20 (6), 599–618.

Alexandrov, P., Ruffet, G., Cheilletz, A., 2002. Muscovite recrystallization and saddle-shaped 40Ar/39Ar age spectra: example from the Blond granite (Massif Central, France). 10Geochimica et Cosmochimica Acta 66, 1793–1807.

Alvarez, W., 1976. A former continuation of the Alps. Geological Society of America Bulletin 87, 891–896.

Fig. 10. Tentative schematic reconstruction of the Alpine geodynamic evolution of the Western Mediterranean area (after Lonergan and White, 1997; Gelabert et al., 2002). Orientation of the extension direction in the Calabrian–Peloritan belt at ~28 Ma from Heymes et al. (2008), based on the paleomagnetic data compiled by Rosenbaum and Lister (2004). Mes: Mesogean oceanic domain; LP: Ligurian–Provencal basin; NA: North-Algerian basin; T: Tyrrhenian Sea; S: Sardinia; C: Corsica; GK: Grande Kabylie; PK: Petite Kabylie; Pe: Peloritan Mountains; CaS: southern Calabria; CaN: northern Calabria.

Please cite this article as: Heymes, T., et al., Alpine tectonics in the Calabrian–Peloritan belt (southern Italy): New $^{40}Ar/^{39}Ar$ data in the Aspromonte Massif area, Lithos (2009), doi:10.1016/j.lithos.2009.10.011

Amodio-Morelli, L., Bonardi, G., Colonna, V., Dietricht, D., Giunta, G., Ippolito, F., Liguori, V., Lorenzoni, S., Paglionico, A., Perrone, V., Piccarretta, G., Russo, M., Scandone, P., Zanettin-Lorenzoni, E., Zuppetta, A., 1976. L'Arco Calabro-Peloritano nell'orogene Appenninico-Maghrebide. Memorie della Società Geologica Italiana 17, 1–60.

Arnaud, N.O., Kelley, S.P., 1995. Evidence for excess argon during high pressure metamorphism in the Dora Maira Massif (Western Alps, Italy), using an ultra-violet laser ablation microprobe 40Ar/39Ar technique. Contributions to Mineralogy and Petrology 21, 249–264.

Arnaud, N.O., Brunel, M., Cantagrel, J.M., Taponnier, P., 1993. High cooling and denudation rates at Konjur Shan, Eastern Pamir (Xinjiang, China) revealed by 40Ar/39Ar alkali feldspar thermochronology. Tectonics 12, 1335–1346.

Atzori, P., del Moro, A., Rottura, A., 1990. Rb/Sr radiometric data from medium- to high-grade metamorphic rocks (Aspromonte nappe) of the north-eastern Peloritani Mountains (Calabrian Arc), Italy. International Journal of Earth Sciences 2, 363–371.

Benedicto, A., Labaume, P., Séguret, M., Séranne, M., 1996. Low-angle crustal ramp and basin geometry in the Gulf of Lion passive margin: Oligocene–Aquitanian Vistrenque graben, SE France. Tectonics 15, 1192–1212.

Bois, C., 1993. Initiation and evolution of the Oligo-Miocene rift basins of southwestern Europe: contribution of deep seismic reflection profiling. Tectonophysics 226, 227–252.

Bonardi, G., Gurrieri, S., Messina, A., Perrone, V., Russo, M., Zuppetta, A., 1979. Osservazioni geologiche e petrografiche sull'Aspromonte. Bolletino della Società Geologica Italiana 98, 55–73.

Bonardi, G., Messina, A., Perrone, V., Russo, M., Russo, S., Zuppetta, A., 1980. Osservazioni sull'evoluzione dell'arco calabro-peloritano nel Miocene inferiore: La Formazione di Stilo-Capo d'Orlando. Bolletino della Società Geologica Italiana 99, 279–309.

Bonardi, G., Compagnoni, R., Messina, A., Perrone, V., 1984a. Riequilibrazioni metamorfiche di probabile età alpina nelle'unità dell'Aspromonte - Arco Calabro-Peloritano. Rendiconti della Società Italiana di Mineralogia e Petrologia 39, 613–628.

Bonardi, G., Messina, A., Perrone, V., Russo, S., Zuppetta, A., 1984b. L'unità di Stilo nel settore meridionale dell'arco Calabro-Peloritano. Bolletino della Società Geologica Italiana 103, 279–309.

Bonardi, G., Compagnoni, R., Del Moro, A., Messina, A., Perrone, V., 1987. Riequilibrazioni tettono-metamorfiche alpine nell'unità dell'Aspromonte, Calabria meridionale. Rendiconti della Società Italiana di Mineralogia e Petrologia 42, 301 Riassunto.

Bonardi, G., Compagnoni, R., Messina, A., Perrone, V., Russo, S., de Francesco, A.M., del Moro, A., Platt, J., 1992. Sovrimpronta metamorfica alpina nell'unità dell'Aspromonte (settore meridionale dell'Arco Calabro-Peloritano). Bolletino della Società Geologica Italiana 111, 81–108.

Bonardi, G., de Capoa, P., di Staso, A., Estévez, A., Martìn-Martìn, M., Martìn-Rojas, I., Perrone, V., Tent-Manclùs, J.E., 2003. Oligocene-to-Early-Miocene depositional and structural evolution of the Calabria-Peloritani Arc southern terrane (Italy) and geodynamic correlations with the Spains Betics and Morocco Rif. Geodinamica Acta 16, 149–169.

Bouillin, J.-P., 1984. Nouvelle interprétation de la liaison Apennin-Maghrébides en Calabre; conséquences sur la paléogéographie téthysienne entre Gibraltar et les Alpes. Revue de Géographie Dynamique et de Géographie Physique 25 (5), 321–338.

Bouillin, J.-P., 1985. Transgression de l'Oligocène inférieur (formation de Palizzi) sur un karst à remplissage bauxitique dans les zones internes calabro-péloritaines (Italie). Comptes-rendus de l'Académie des Sciences, Paris 301, 415–420.

Bouillin, J.-P., 1986. Le «bassin maghrébin»: une ancienne limite entre l'Europe et l'Afrique à l'ouest des Alpes. IIBulletin de la Société géologique de France 8, 547–558.

Bouillin, J.-P., Bellomo, D., 1990. Les filons sédimentaires jurassiques de Longobucco-Cavoleto (Calabre, Italie); application à l'étude des paléostructures d'une marge téthysienne. Geodinamica Acta 4, 111–120.

Bouillin, J.-P., Majesté-Menjoulas, C., Baudelot, S., Cygan, C., Fournier-Vinas, C., 1987. Les formations paléozoïques de l'arc calabro-péloritain dans leur cadre structural. Bolletino della Società Geologica Italiana 106, 693–698.

Bouillin, J.-P., Mouterde, R., Olivier, P., Majesté-Menjoulas, C., 1988. Le Jurassique de Longobucco (Calabre, Italie), à la jonction de la Téthys ligure et de la Téthys maghrébine. Bulletin de la Société géologique de France 8, 93–103.

Bouillin, J.-P., Dumont, T., Olivier, P., 1992. Organisation structurale et sédimentaire de la paléomarge nord téthysienne au Jurassique dans les monts Péloritains (Sicile, Italie). Bulletin de la Société géologique de France 163 (6), 761–770.

Bouillin, J.-P., Poupeau, G., Tricart, P., Bigot-Cormier, F., Mascle, G., Torelli, L., 1998. Premières données thermochronologiques sur les socles sarde et kabylo-péloritain submergés dans le canal de Sardaigne. Comptes-rendus de l'Académie des Sciences, Paris 326, 561–566.

Bouillin, J.-P., Dumont, T., Mouterde, R., Somma, R., Hippolyte, J.-C., 1999. Un escarpement sous-marin permanent du Lias à l'Eocène dans la dorsale calcaire péloritaine (Sicile, Italie). Comptes-rendus de l'Académie des Sciences, Paris 328, 347–352.

Bruguier, O., Hammor, D., Bosch, D., Caby, R., 2009. Miocene incorporation of peridotite into the Hercynian basement of the Maghrebides (Edough massif, NE Algeria): implications for the geodynamic evolution of the Western Mediterranean. Chemical Geology 261 (1–2), 171–183.

Brunet, C., Monié, P., Jolivet, L., Cadet, J.-P., 2000. Migration of compression and extension in the Tyrrhenian Sea, insights from 40Ar/39Ar ages on micas along a transect from Corsica to Tuscany. Tectonophysics 321, 127–155.

Burgess, R., Kelley, S.P., Parsons, I., Walker, F.D.L., Worden, R.H., 1992. 40Ar/39Ar analysis of Perthite microtextures and fluid inclusions in alkali feldspars from the Klokken Syenite, South Greenland. Earth and Planetary Science Letters 109, 147–167.

Caby, R., Hammor, D., Delor, C., 2001. Metamorphic evolution, partial melting and Miocene exhumation of lower crust in the Edough metamorphic core complex, west Mediterranean orogen, eastern Algeria. Tectonophysics 342 (3–4), 239–273.

Cello, G., Invernizzi, C., Mazzoli, S., 1996. Structural signature of tectonic processes in the Calabrian Arc, southern Italy. Evidence from the oceanic-derived Diamante-Terranova Unit. Tectonics 15, 187–200.

Cirrincione, R., Pezzino, A., 1993. Nuovi dati struturali sulle successioni mesozoiche metamorfiche dei Monti Peloritani orientali. Bolletino della Società Geologica Italiana 13, 195–203.

Cirrincione, R., Ortolano, G., Pezzino, A., Punturo, R., 2008. Poly-orogenic multi-stage metamorphic evolution inferred via P–T pseudosections: an example from Aspromonte Massif basement rocks (Southern Calabria, Italy). Lithos 103 (3–4), 466–502.

Dahl, P.S., 1996. The crystal-chemical basis for Ar retention in micas: inferences from interlayer partitioning and implications for geochronology. Contributions to Mineralogy and Petrology 123, 22–39.

De Gregorio, S., Rotolo, S.G., Villa, I.M., 2003. Geochronology of the medium to high-grade metamorphic units of the Peloritani Mts., Sicily. International Journal of Earth Sciencs 92, 852–872.

Del Moro, A., Pardini, G., Maccarrone, E., Rottura, A., 1982. Studio radiometrico Rb–Sr di granitoidi peraluminosi dell'arco Calabro-Peloritano. Rendiconti della Società Italiana di Mineralogia e Petrologia 38 (3), 1015–1026.

Del Moro, A., Fornelli, A., Piccarreta, G., 2000. Tectonothermal history of the Hercynian continental crust of the Serre (southern Calabria, Italy) monitored by Rb–Sr biotite resetting. Terra Nova 12, 239–244.

Dewey, J.F., Helman, M.L., Turco, E., Hutton, D.H.W., Knott, S.D., 1989. Kinematics of the Western Mediterranean. Alpine Tectonics. GSSP 45, 265–283.

Dietricht, D., 1988. Sense of overthrust shear in the Alpine nappes of Calabria (Southern Italy). Journal of Structural Geology 10 (4), 373–381.

Doglioni, C., Gueguen, E., Sàbat, F., Fernandez, M., 1997. The western Mediterranean extensional basins and the Alpine orogen. Terra Nova 9, 109–112.

Dubois, R., 1970. Phases de serrage, nappes de socle et métamorphisme alpin à la jonction Calabre-Apennin: la suture calabro-apenninique. Revue de Géographie Dynamique et de Géographie Physique 12 (3), 221–254.

Dunlap, W.J., 1997. Neocrystallization or cooling? 40Ar/39Ar ages of white micas from low-grade mylonites. Chemical Geology 143, 181–203.

Faccenna, C., Becker, T.W., Lucente, F.P., Jolivet, L., Rossetti, F., 2001. History of subduction and back-arc extension in the Central Mediterranean. Geophysical Letters 145, 809–820.

Faccenna, C., Speranza, F., Caracciolo, F.D., Mattei, M., Oggiano, G., 2002. Extensional tectonics on Sardinia (Italy): insights into the arc back-arc transitional regime. Tectonophysics 356 (4), 213–232.

Faccenna, C., Piromallo, C., Crespo-Blanc, A., Jolivet, L., Rossetti, F., 2004. Lateral slab deformation and the origin of the western Mediterranean arcs. Tectonics 23, TC1012.

Fiannacca, P., Williams, I.S., Cirrincione, R., Pezzino, A., 2008. Crustal contributions to Late-Hercynian peraluminous magmatism in the Southern Calabria–Peloritani Orogen, Southern Italy: petrogenetic inferences and the Gondwana connection. Journal of Petrology 49, 1497–1514.

Gelabert, B., Sàbat, F., Rodriguez-Perea, A., 2002. A new proposal for the Late Cenozoic geodynamic evolution of the Western Mediterranean. Terra Nova 14, 93–100.

Graessner, T., Schenk, V., 1999. Low-pressure metamorphism of Paleozoic pelites in the Aspromonte, southern Calabria: contraints for the thermal evolution in the Calabrian crustal cross-section during Hercynian orogeny. Journal of metamorphic Geology 17, 157–172.

Graessner, T., Schenk, V., Bröcker, M., Mezger, K., 2000. Geochronological constraints on the timing of granitoid magmatism, metamorphism and post-metamorphic cooling in the Hercynian crustal cross-section of Calabria. Journal of metamorphic Geology 18, 409–421.

Grande, A., Di Vincenzo, G., Prosser, G., Caggianelli, A., 2009. Direct evidence of Middle Oligocene extension in the Calabria–Peloritani terrane from co-seismic faulting: the pseudotachylyte-bearing shear zones of Palmi (southern Calabria, Italy). Terra Nova 21 (4), 293–303.

Gueguen, E., Doglioni, C., Fernandez, M., 1998. On the post-25 Ma geodynamic evolution of the western Mediterranean. Tectonophysics 298 (1–3), 259–269.

Gutscher, M.A., et al., 2002. Evidence for active subduction beneath Gibraltar. Geology 30, 1071–1074.

Hames, W.E., Bowring, S.A., 1994. An empirical evaluation of the argon diffusion geometry in muscovite. Earth and Planetary Science Letters 124, 161–167.

Harrison, T.M., McDougall, I., 1981. Excess 40Ar in metamorphic rocks from the Broken Hill, New South Wales: implications for 40Ar/39Ar age spectra and the thermal history of the region. Earth and Planetary Science Letters 55, 123–149.

Harrison, T.M., Heizler, M.T., Lovera, O.M., Wenji, C., Grove, M., 1994. A chlorine disinfectant for excess argon released from K-feldspar during step heating. Earth and Planetary Science Letters 123, 95–104.

Heizler, M.T., Ralser, S., Karlstrom, K.E., 1997. Late Proterozoic (Grenville?) deformation in central New Mexico determined from single-crystal muscovite 40Ar/39Ar age spectra. Precambrian Research 84, 1–15.

Heymes, T., Bouillin, J.P., Pêcher, A., Monié, P., Compagnoni, R., 2008. Middle Oligocene extension in the Mediterranean Calabro–Peloritan belt (southern Italy): insights from the Aspromonte nappes-pile. Tectonics 27, TC2006.

Hippolyte, J.-C., Angelier, J., Bergerat, F., Nury, D., Guieu, G., 1993. Tectonic–stratigraphic record of paleostress time changes in the Oligocene basins of the Provence, southern France. Tectonophysics 226, 15–35.

Jolivet, L., Faccenna, C., 2000. Mediterranean extension and the Africa–Eurasia collision. Tectonics 19, 1095–1106.

Please cite this article as: Heymes, T., et al., Alpine tectonics in the Calabrian–Peloritan belt (southern Italy): New $^{40}Ar/^{39}Ar$ data in the Aspromonte Massif area, Lithos (2009), doi:10.1016/j.lithos.2009.10.011

Jolivet, L., Faccenna, C., Goffé, B., Mattei, M., Rossetti, F., Brunet, C., Storti, F., Funiciello, R., Cadet, J.-P., d'Agostino, N., Parra, T., 1998. Midcrustal shear zones in postorogenic extension: example from the northern Tyrrhenian Sea. Journal of Geophysical Research 103, 12123–12160.

Jourdan, F., Renne, P.R., 2007. Age calibration of the Fish Canyon sanidine 40Ar/39Ar dating standard using primary K–Ar standards. Geochimica et Cosmochimica Acta 71 (2), 387–402.

Kastens, K., Mascle, J., Auroux, C., Bonatti, E., Broglia, C., Channell, J., Curzi, P., Emeis, K., Glaçon, G., Hasegawa, S., Hieke, W., Mascle, G., McCoy, F., McKenzie, J., Mendelson, J., Mûller, C., Rehault, J.-P., Robertson, A., Sartori, R., Sprovieri, R., Torii, M., 1988. ODP Leg 107 in the Tyrrhenian Sea: insights into passive margin and back-arc basin evolution. Geological Society of America Bulletin 100, 1140–1156.

Knott, S.D., 1987. The Liguride Complex of Southern Italy, a Cretaceous to Paleogene accretionnary wedge. Tectonophysics 142, 217–226.

Langone, A., Gueguen, E., Prosser, G., Caggianelli, A., Rottura, A., 2006. The Curinga-Girifalco fault zone (northern Serre, Calabria) and its significance within the Alpine tectonic evolution of the western Mediterranean. Journal of Geodynamics 42 (4–5), 140–158.

Lanphere, M.A., Baadsgaard, H., 2001. Precise K-Ar, 40Ar/39Ar, Rb–Sr, and U–Pb mineral ages from the 27.5 Ma Fish Canyon Tuff reference standard. Chemical Geology 175, 655–671.

Leake, B.E., Wooley, A.R., Birch, W.D., Burke, E.A.J., Ferraris, G., Grice, J.D., Hawthorne, F.C., Kisch, H.J., Krivovichev, V.G., Schumacher, J.C., Stephenson, N.C.N., Whittaker, E.J.W., 2004. Nomenclature of amphiboles: additions and revisions to the International Mineralogical Association's amphibole nomenclature. Mineralogical Magasine 68, 209–215.

Li, S., Wang, S., Chen, Y., Liu, D., Qiu, J., Zhou, H., Zhang, Z., 1994. Excess argon in phengite from eclogite evidence from dating of eclogite minerals by Sm–Nd, Rb–Sr and 40Ar/ 39Ar methods. Chemical Geology 112, 343–350.

Liberi, F., Morten, L., Piluso, E., 2006. Geodynamic significance of ophiolites within the Calabrian Arc. Island Arc 15, 26–43.

Lonergan, L., White, N., 1997. Origin of the Betic-Rif mountain belt. Tectonics 16, 504–522.

Lovera, O.M., Richter, F.M., Harrison, T.M., 1989. The 40Ar/39Ar thermochronometry for slowly cooled samples having a distribution of diffusion domain sizes. Journal of Geophysical Research 94, 17,917–17,935.

Lovera, O.M., 1992. Computer programs to model 40Ar/39Ar diffusion data from multidomain samples. Computers and Geosciences 18, 789–813.

Lucente, F.P., Chiarabba, C., Cimini, G.B., Giardini, D., 1999. Tomographic constraints on the geodynamic evolution of the Italian region. Journal of Geophysical Research 104, 20307–20327.

Lucente, F.P., Margheriti, L., Piromallo, C., Barruol, G., 2006. Seismic anisotropy reveals the long route of the slab through the western–central Mediterranean mantle. Earth and Planetary Science Letters 241 (3–4), 517–529.

Lustrino, M., Morra, V., Fedele, L., Serracino, M., 2007. The transition between 'orogenic' and 'anorogenic' magmatism in the western Mediterranean area: the Middle Miocene volcanic rocks of Isola del Toro (SW Sardinia, Italy). Terra Nova 19 (2), 148–159.

Malinverno, A., Ryan, W.B.F., 1986. Extension in the Tyrrhenian Sea and shortening in the Apennines as result of arc migration driven by sinking of the lithosphere. Tectonics 5 (2), 227–245.

Mascle, G.H., Tricart, P., Torelli, L., Bouillin, J.P., Rolfo, F., Lapierre, H., Monié, P., Depardon, S., Mascle, J., Peis, D., 2001. Evolution of the Sardinia Channel (Western Mediterranean): new constraints from a diving survey on Cornacya seamount off SE Sardinia. Marine Geology 179 (3–4), 179–201.

Mascle, G.H., Tricart, P., Torelli, L., Bouillin, J.-P., Compagnoni, R., Depardon, S., Mascle, J., Pêcher, A., Peis, D., Rekhiss, F., Rolfo, F., Bellon, H., Brocard, G., Lapierre, H., Monié, P., Poupeau, G., 2004. Structure of the Sardinia Channel: crustal thinning and tardi-orogenic extension in the Apennic-Maghrebian orogen; results of the Cyana submersible survey (SARCYA & SARTUCYA) in the western Mediterranean. Bulletin de la Société géologique de France 175 (6), 607–627.

Massonne, H.-J., Schreyer, W., 1987. Phengite geothermobarometry based on the limiting assemblage with K-felspar, phlogopite, and quartz. Contributions to Mineralogy and Petrology 96, 212–224.

Maurel, O., Monié, P., Respaut, J.P., Leyreloup, A.F., Maluski, H., 2003. Pre-metamorphic 40Ar/39Ar and U–Pb ages in HP metagranitoids from the Hercynian belt (France). Chemical Geology 193, 195–214.

McDougall, I., Harrison, T.M., 1999. Geochronology and Thermochronology by 40Ar/ 39Ar Method, 2nd Ed. Oxford University Press, New York.

McLaren, S., Reddy, S., 2008. Automated mapping of K-feldspar by electron backscatter diffraction and application to 40Ar/39Ar dating. Journal of Structural Geology 30, 1229–1241.

Messina, A., Compagnoni, R., de Francesco, A.M., Russo, S., 1992. Alpine metamorphic overprint in the crystalline basement of the Aspromonte Unit (Calabrian–Peloritan arc – southern Italy). IGCP 276 (5), 353–379.

Micheletti, F., Barbey, P., Fornelli, A., Piccarreta, G., Deloule, E., 2007. Latest Precambrian to Early Cambrian U–Pb zircon ages of augen gneisses from Calabria (Italy), with inference to the Alboran microplate of the peri-Gondwana terranes. International Journal of Earth Sciences 96, 843–860.

Monié, P., 1990. Preservation of Hercynian 40Ar/39Ar ages through high-pressure low-temperature Alpine metamorphism in the Western Alps. European Journal of Mineralogy 2, 343–361.

Monié, P., Maluski, H., Saadallah, A., Caby, R., 1988. New 39Ar–40Ar ages of Hercynian and Alpine thermotectonic events in Grande Kabylie (Algeria). Tectonophysics 152, 53–69.

Mulch, A., Cosca, M.A., 2004. Recrystallization or cooling ages: in situ UV-laser 40Ar/ 39Ar geochronology of muscovite in mylonitic rocks. Journal of the Geological Society London 161, 573–582.

Ogniben, L., 1973. Schema geologico della Calabria in base ai dati odierni. Geologica Romana 12, 243–585.

Ortolano, G., Cirrincione, R., Pezzino, A., 2005. P–T evolution of Alpine metamorphism in the southern Aspromonte Massif (Calabria — Italy). Schweizerische Mineralogische und Petrographische Mitteilungen 85, 31–56.

Parsons, I., Brown, W.L., 1988. Sidewall crystallization in the Klokken intrusion: zoned ternary feldspars and coexisting minerals. Contributions to Mineralogy and Petrology 98, 431–443.

Pezzino, A., Puglisi, G., 1980. Indagine geologico-petrografica sul cristallino dell'Aspromonte centro-settentrionale (Calabria). Bolletino della Società Geologica Italiana 99, 255–268.

Pezzino, A., Pannucci, S., Puglisi, G., Atzori, P., Ioppolo, S., Lo Giudice, A., 1990. Geometry and metamorphic environment of the contact betwenn the Aspromonte–Peloritani Unit (Upper Unit) and the Madonna di Polsi Unit (Lower Unit) in the Central Aspromonte area (Calabria). Bolletino della Società Geologica Italiana 109, 455–469.

Pezzino, A., Puglisi, G., Pannucci, S., Ioppolo, S., 1992. Due unità cristalline a grado metamorfico diverso in Aspromonte centrale. Geometrica dei loro rapporti, ambientazione metamorfica del loro contatto e caratteri petrografici delle metamorfiti. Bolletino della Società Geologica Italiana 111, 69–80.

Platt, J.P., 2007. From orogenic hinterlands to Mediterranean-style back-arc basins: a comparative analysis. Journal of the Geological Society, London 164, 297–311.

Platt, J.P., Compagnoni, R., 1990. Alpine ductile deformation and metamorphism in a calabrian basement nappe (Aspromonte, south Italy). Eclogae geologicae Helvetiae 83 (1), 41–58.

Rehault, J.-P., Boillot, G., Mauffret, A., 1984. The western mediterranean basin geological evolution. Marine Geology 55, 447–477.

Roda, C., 1965. Il calcare portlandiano a Dasycladaceae di M. Mutolo (Reggio Calabria). Geologica Romana 4, 259–290.

Rollet, N., Deverchère, J., Beslier, M.-O., Guennoc, P., Rehault, J.-P., Sosson, M., Truffert, C., 2002. Back arc extension, tectonic inheritance, and volcanism in the Ligurian Sea, Western Mediterranean. 3Tectonics 21, TC900027.

Rosenbaum, G., Lister, G.S., 2004. Neogene and quaternary rollback evolution of the Tyrrhenian Sea, the Apennines, and the Sicilian Maghrebides. Tectonics 23, TC1013.

Rosenbaum, G., Lister, G.S., Duboz, C., 2002. Relative motions of Africa, Iberia and Europe during Alpine orogeny. Tectonophysics 359 (1–2), 117–129.

Rossetti, F., Faccenna, C., Goffé, B., Monié, P., Argentieri, A., Funiciello, R., Mattei, M., 2001. Alpine structural and metamorphic signature of the Sila Piccola Massif nappe stack (Calabria, Italy): insights for the tectonic evolution of the Calabrian Arc. Tectonics 20 (1), 112–133.

Rossetti, F., Goffé, B., Monié, P., Faccenna, C., Vignaroli, G., 2004. Alpine orogenic P–T-t-deformation history of the Catena Costiera area and surrounding regions (Calabria Arc, southern Italy): the nappe edifice of north Calabria revised with insights on the Tyrrhenian–Apennine system formation. Tectonics 23, TC6011.

Royden, L.H., 1993. Evolution of retreating subduction boundaries formed during continental collision. Tectonics 12, 629–638.

Saadallah, A., Caby, R., 1996. Extensional detachment tectonics in the Grande Kabylie metamorphic core complex of the Maghrebides (northern Algeria). Tectonophysics 267, 257–274.

Samson, S.D., Alexander, E.C.J., 1987. Calibration of the interlaboratory 40Ar–39Ar dating standard, MMhb-1. Chemical geology 66, 27–34.

Schenk, V., 1980. U–Pb and Rb–Sr radiometric dates and their correlation with metamorphic events in the granulite-facies basement of the Serre, southern Calabria (Italy). Contributions to Mineralogy and Petrology 73, 23–38.

Schettino, A., Turco, E., 2006. Plate kinematics of the Western Mediterranean region during the Oligocene and Early Miocene. Geophysical Journal International 166 (3), 1398–1423.

Scheuber, E., Hammerschmidt, K., Friedrichsen, H., 1995. 40Ar/39Ar and Rb–Sr analyses from ductile shear zones from the Atacama Fault Zone, northern Chile: the age of deformation. Tectonophysics 250, 61–87.

Seranne, M., 1999. The Gulf of Lion continental margin (NW Mediterranean) revisited by IBS: an overview. In: Durand, B., Jolivet, L., Horvath, F., Seranne, M. (Eds.), The Mediterranean Basins: Tertiary Extension within the Alpine Orogen: Geological Society, London, Special Publications, 156, pp. 15–36.

Somma, R., Messina, A., Mazzoli, S., 2005. Syn-orogenic extension in the Peloritani Alpine Thrust Belt (NE Sicily, Italy): evidence from the Alì Unit. Comptes-Rendus Geoscience 337, 861–871.

Stampfli, G.M., Mosar, J., Marquer, D., Marchant, R., Baudin, T., Borel, G., 1998. Subduction and obduction processes in the Swiss Alps. Tectonophysics 296 (1–2), 159–204.

Thomson, S.N., 1994. Fission track analysis of the crystalline basement rocks of the Calabrian Arc, southern Italy: evidence of Oligo-Miocene late-orogenic extension and erosion. Tectonophysics 238, 331–352.

Trombetta, A., Cirrincione, R., Corfu, F., Mazzoleni, P., Pezzino, A., 2004. Mid-Ordovician U–Pb ages of porphyroids in the Peloritan Mountains (NE Sicily): palaeogeographical implications for the evolution of the Alboran microplate. Journal of the Geological Society, London 161, 265–276.

Turner, G., 1971. 40Ar/39Ar dating: the optimization of irradiation parameters. Earth and Planetary Science Letters 10, 227–234.

Vidal, O., Parra, T., 2000. Exhumation paths of high-pressure metapelites obtained from local equilibria for chlorite–phengite assemblages. Geological Journal 35, 139–161.

Vigliotti, L., Langenheim, V.E., 1995. When did Sardinia stop rotating — new paleomagnetic results. Terra Nova 7 (4), 424–435.

Villa, I.M., 1998. Isotopic closure. Terra Nova 10, 42–47.

Villa, I.M., Ruggieri, G., Puxeddu, M., 1997. Petrological and geochronological discrimination of two white-mica generations in a granite cored from the Larderello-Travale geothermal field (Italy). European Journal of Mineralogy 9, 563–568.

Please cite this article as: Heymes, T., et al., Alpine tectonics in the Calabrian–Peloritan belt (southern Italy): New $^{40}Ar/^{39}Ar$ data in the Aspromonte Massif area, Lithos (2009), doi:10.1016/j.lithos.2009.10.011

Weltje, G., 1992. Oligocene to Early Miocene sedimentation and tectonics in the southern part of the Calabrian–Peloritan Arc (Aspromonte, southern Italy): a record of mixed-mode piggy-back basin evolution. Basin Research 4, 37–68.

Westphal, M., Orsini, J., Vellutini, P., 1976. Corsica–Sardinia microcontinent, its initial position — paleomagnetic data and geological fitting. Tectonophysics 30 (1–2), 141–157.

Wijbrans, J.R., McDougall, I., 1986. 40Ar/39Ar dating of white micas from an alpine high-pressure metamorphic belt on Naxos (Greece): the resetting of the argon isotopic system. Contributions to Mineralogy and Petrology 93, 187–194.

Worley, B., Powell, R., Wilson, C.J.L., 1997. Crenulation cleavage formation; evolving diffusion, deformation and equilibration mechanisms with increasing metamorphic grade. Journal of Structural Geology 19, 1121–1135.

York, D., 1969. Least squares fitting of a straight line with correlated errors. Earth and Planetary Science Letters 5, 320–324.

Please cite this article as: Heymes, T., et al., Alpine tectonics in the Calabrian–Peloritan belt (southern Italy): New $^{40}Ar/^{39}Ar$ data in the Aspromonte Massif area, Lithos (2009), doi:10.1016/j.lithos.2009.10.011